Article

c-Jun overexpression in CAR T cells induces exhaustion resistance

https://doi.org/10.1038/s41586-019-1805-z

Received: 7 September 2018

Accepted: 17 October 2019

Published online: 4 December 2019

Rachel C. Lynn[1,11], Evan W. Weber[1,13], Elena Sotillo[1,13], David Gennert[2], Peng Xu[1], Zinaida Good[1,3,4], Hima Anbunathan[1], John Lattin[1], Robert Jones[1], Victor Tieu[1], Surya Nagaraja[5], Jeffrey Granja[2], Charles F. A. de Bourcy[6,12], Robbie Majzner[7], Ansuman T. Satpathy[2,4], Stephen R. Quake[6,8], Michelle Monje[1,5,7], Howard Y. Chang[2,4,9] & Crystal L. Mackall[1,4,7,10]*

Chimeric antigen receptor (CAR) T cells mediate anti-tumour effects in a small subset of patients with cancer[1–3], but dysfunction due to T cell exhaustion is an important barrier to progress[4–6]. To investigate the biology of exhaustion in human T cells expressing CAR receptors, we used a model system with a tonically signaling CAR, which induces hallmark features of exhaustion[6]. Exhaustion was associated with a profound defect in the production of IL-2, along with increased chromatin accessibility of AP-1 transcription factor motifs and overexpression of the bZIP and IRF transcription factors that have been implicated in mediating dysfunction in exhausted T cells[7–10]. Here we show that CAR T cells engineered to overexpress the canonical AP-1 factor c-Jun have enhanced expansion potential, increased functional capacity, diminished terminal differentiation and improved anti-tumour potency in five different mouse tumour models in vivo. We conclude that a functional deficiency in c-Jun mediates dysfunction in exhausted human T cells, and that engineering CAR T cells to overexpress c-Jun renders them resistant to exhaustion, thereby addressing a major barrier to progress for this emerging class of therapeutic agents.

CAR-expressing T cells demonstrate impressive response rates in B cell malignancies, but fewer than 50% of patients experience long-term disease control[11,12] and CAR T cells have not mediated sustained responses in solid tumours[3]. Several factors limit the efficacy of CAR T cells, including a requirement for high antigen density for optimal CAR function enabling rapid selection of antigen loss or antigen low variants[12–14], the suppressive tumour microenvironment[15] and intrinsic T cell dysfunction due to T cell exhaustion[6,11,16]. T cell exhaustion has been increasingly incriminated as a cause of CAR T cell dysfunction[6,11,16,17], raising the prospect that engineering exhaustion-resistant CAR T cells could improve clinical outcomes.

T cell exhaustion is characterized by high expression of inhibitory receptors and widespread transcriptional and epigenetic alterations[4,5,7,18,19], but the mechanisms responsible for impaired function in exhausted T cells are unknown. Blockade of PD-1 can reinvigorate some exhausted T cells[20] but does not restore function fully, and trials using PD-1 blockade in combination with CAR T cells have not demonstrated efficacy[21]. Using a model in which healthy T cells are driven to exhaustion by the expression of a tonically signalling CAR, exhausted human T cells demonstrated widespread epigenomic dysregulation of AP-1 transcription factor-binding motifs and increased expression of the bZIP and IRF transcription factors that have been implicated in the regulation of exhaustion-related genes. Therefore, we tested the hypothesis that dysfunction in this setting resulted from an imbalance between activating and immunoregulatory AP-1–IRF complexes by inducing overexpression of c-Jun—an AP-1 family transcription factor associated with productive T cell activation. Consistent with this hypothesis, overexpression of c-Jun rendered CAR T cells resistant to exhaustion, as demonstrated by enhanced expansion potential in vitro and in vivo, increased functional capacity, diminished terminal differentiation and improved anti-tumour potency in multiple in vivo models.

HA-28z CAR rapidly induces T cell exhaustion

Exhaustion in human T cells was recently demonstrated after expression of a CAR incorporating the disialoganglioside (GD2)-specific 14g2a scFv, CD3ζ and CD28 signalling domains (GD2-28z), as a result of tonic signalling mediated via antigen-independent aggregation[6]. Here we show that CARs incorporating the 14g2a-E101K scFv, which demonstrate higher affinity for GD2[22] (HA-28z), display a more severe exhaustion phenotype (Extended Data Fig. 1a–c). In contrast to CD19-28z CAR T cells (without tonic signalling), HA-28z CAR T cells develop profound features of exhaustion, including reduced expansion in culture, increased expression of inhibitory receptors, exaggerated effector differentiation, and diminished IFNγ and markedly decreased IL-2 production after stimulation (Fig. 1a–d, Extended Data Fig. 1d, e). The

[1]Stanford Cancer Institute, Stanford University School of Medicine, Stanford, CA, USA. [2]Center for Personal Dynamic Regulomes, Stanford University, Stanford, CA, USA. [3]Department of Biomedical Data Science, Stanford University, Stanford, CA, USA. [4]Parker Institute for Cancer Immunotherapy, San Francisco, CA, USA. [5]Department of Neurology, Stanford University, Stanford, CA, USA. [6]Departments of Bioengineering and Applied Physics, Stanford University, Stanford, CA, USA. [7]Department of Pediatrics, Stanford University School of Medicine, Stanford, CA, USA. [8]Chan Zuckerberg Biohub, San Francisco, CA, USA. [9]Howard Hughes Medical Institute, Stanford University, Stanford, CA, USA. [10]Department of Medicine, Stanford University School of Medicine, Stanford, CA, USA. [11]Present address: Lyell Immunopharma, South San Francisco, CA, USA. [12]Present address: Chan Zuckerberg Initiative, San Francisco, CA, USA. [13]These authors contributed equally: Evan W. Weber, Elena Sotillo. *e-mail: cmackall@stanford.edu

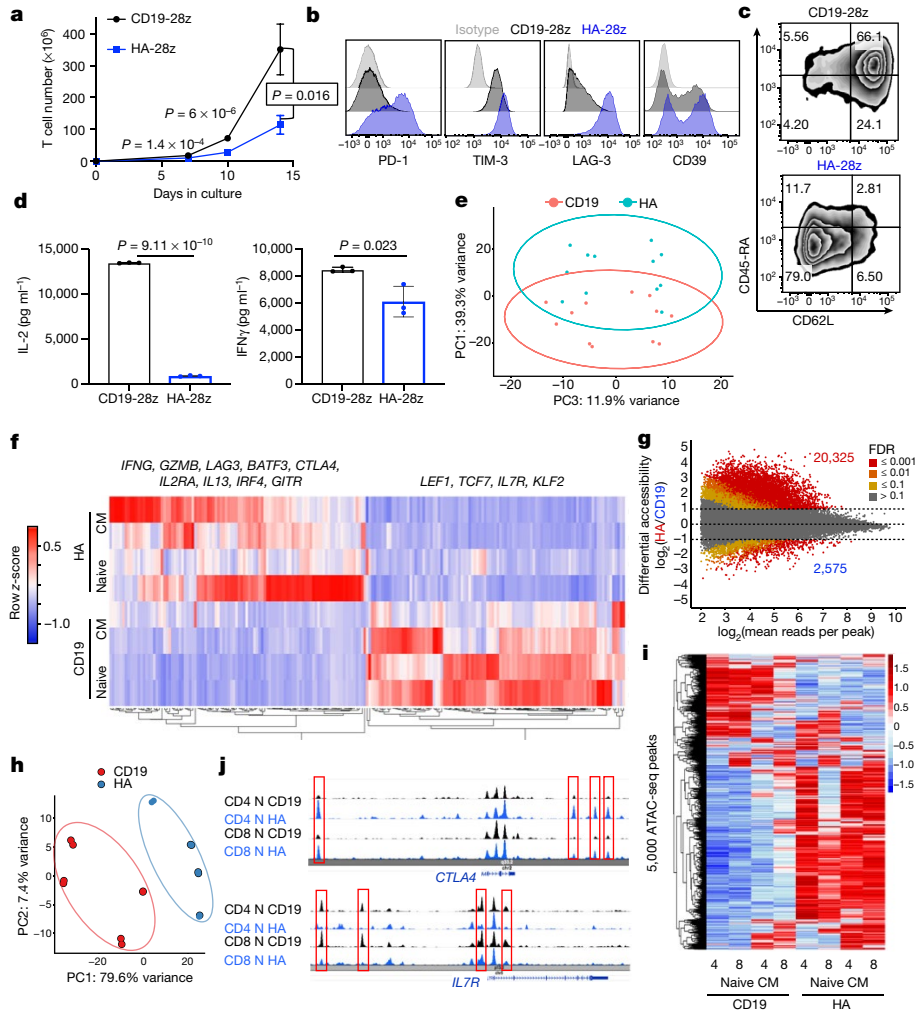

Fig. 1 | HA-28z CAR T cells manifest phenotypic, functional, transcriptional and epigenetic hallmarks of T cell exhaustion. a, Primary T cell expansion. Data are mean ± s.e.m. from $n = 10$ independent experiments. **b**, Surface expression of exhaustion-associated markers. **c**, Surface expression of CD45RA and CD62L to distinguish T memory stem cells ($CD45RA^+CD62L^+$), central memory cells ($CD45RA^-CD62L^+$), and effector memory cells ($CD45RA^-CD62L^-$). **d**, IL-2 (left) and IFNγ (right) release after 24-h co-culture with $CD19^+GD2^+$ Nalm6-GD2 leukaemia cells. Data are mean ± s.d. from triplicate wells. In **b**–**d**, one representative donor (of $n = 10$ experiments) is shown for each assay. *P* values determined by unpaired two-tailed *t*-tests. **e**, Principal component analysis (PCA) of global transcriptional profiles of naive- and central-memory-derived CD19-28z (CD19) or HA-28z (HA) CAR T cells at days 7, 10 and 14 in culture. PC1 (39.3% variance) separates CD19-28z from HA-28z CAR T cells. **f**, Gene expression of the top 200 genes driving PC1. Genes of interest in each cluster are listed. **g**, Differentially accessible chromatin regions (peaks) in $CD8^+$ CD19-28z and HA-28z CAR T cells. Both naive and central memory cell subsets are incorporated for each CAR. **h**, PCA of ATAC-seq chromatin accessibility in CD19-28z or HA-28z CAR T cells. PC1 (76.9% variance) separates CD19-28z from HA-28z CAR samples. **i**, Global chromatin accessibility profile of $CD4^+$ and $CD8^+$ CD19-28z and HA-28z CAR T cells derived from naive (N) and central memory (CM) subsets. Top 5,000 peaks. **j**, Differentially accessible enhancer regions in CD19- and HA-28z CAR T cells in the *CTLA4* (top) or *IL7R* (bottom) loci. Unless noted otherwise, all analyses were done on day 10 of culture. *GITR* is also known as *TNFRSF18*.

functional defects are due to exhaustion-associated dysfunction rather than suboptimal interaction of the HA-28z CAR with its target GD2, because they are also observed in CD19-28z CAR T cells when HA-28z CAR is co-expressed using a bi-cistronic vector (Extended Data Fig. 1f). Principal component analysis (PCA) of RNA-sequencing (RNA-seq) data demonstrated that the strongest driver of transcriptional variance was the presence of the exhausting HA-28z versus control CD19-28z CAR (Fig. 1e), although some cell-type-specific differences were observed (Extended Data Fig. 1g).

The top 200 most differentially expressed genes (Fig. 1f, Supplementary Table 1) included activation-associated genes (*IFNG*, *GZMB* and *IL2RA*), inhibitory receptors (*LAG3* and *CTLA4*) and inflammatory chemokines or cytokines (*CXCL8*, *IL13* and *IL1A*), and genes associated with naive and memory T cells (*IL7R*, *TCF7*, *LEF1* and *KLF2*), which overlapped with gene sets described in chronic lymphocytic choriomeningitis virus (LCMV) mouse models[4] (Extended Data Fig. 1h). Single-cell RNA-seq analysis of GD2-28z versus CD19-28z CAR T cells revealed similar differential gene expression as HA-28z CAR T cells (Extended Data Fig. 2).

T cell exhaustion is associated with widespread epigenetic changes[18,20]. Using ATAC-seq (assay for transposase-accessible chromatin using sequencing) analysis[23] (Fig. 1g, Extended Data Figs. 3, 4a), we observed that $CD8^+$ HA-28z CAR T cells displayed more than 20,000 unique differentially accessible chromatin regions (peaks) compared with less than 3,000 unique peaks in $CD8^+$ CD19-28z CAR T cells (false discovery rate (FDR) < 0.1 and $\log_2$-transformed fold change > 1). Principal component analysis (PCA) revealed HA-28z versus CD19-28z CAR as the strongest driver of differential chromatin states (PC1 variance 79.6%, Fig. 1h), with weaker but observable differences observed between naive and central memory cells (PC2 variance 7.4%), and CD4 versus CD8 subsets (PC3 variance 6.5%; Extended Data Fig. 4b). Clustering the top 5,000 differentially accessible regions revealed a similar epigenetic

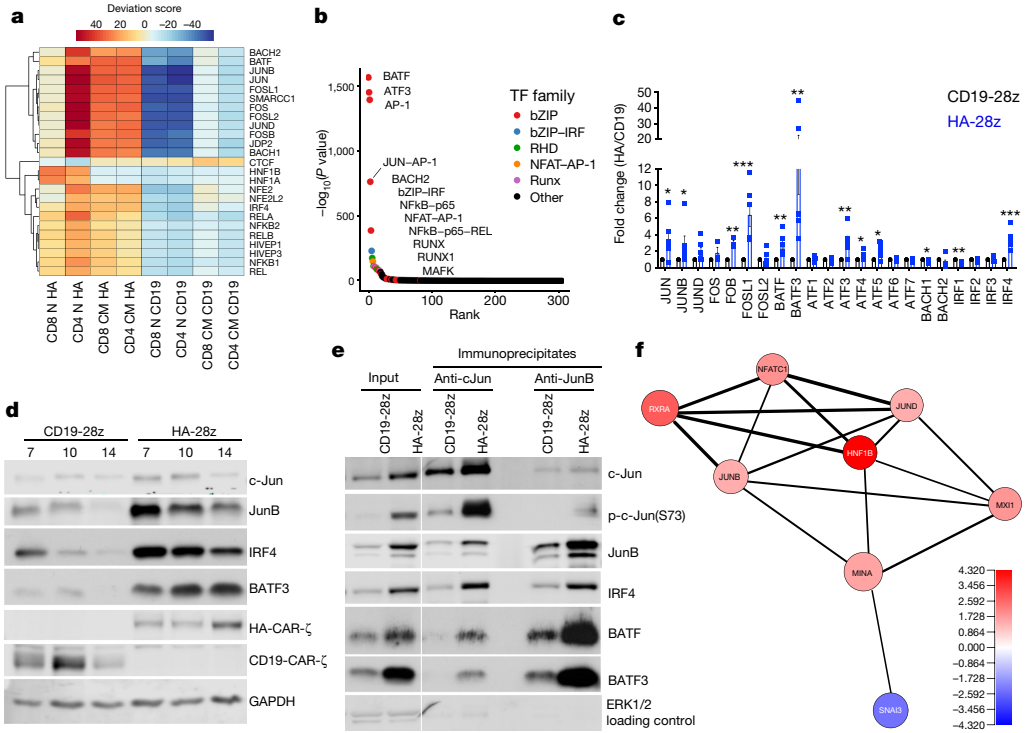

Fig. 2 | AP-1 family signature in exhausted CAR T cells. a, Top 25 transcription factor motif deviation scores in day 10 HA-28z (HA) versus CD19-28z (CD19) CAR T cells by chromVAR analysis. **b**, Top transcription factor (TF) motifs enriched in naive CD8$^+$ HA-28z CAR T cells. **c**, Bulk RNA-seq expression (fold change HA/CD19) of indicated AP-1–bZIP and IRF family members in CD19-28z (black) and HA-28z (blue) CAR T cells. Data are mean ± s.e.m. from $n = 6$ samples across three donors. $^*P < 0.05$, $^{**}P < 0.01$, $^{***}P < 0.001$, two-tailed ratio *t*-tests (see Supplementary Information for exact *P* values). **d**, Increased protein expression of c-Jun, JunB, BATF3 and IRF4 in HA-28z versus CD19-28z CAR T cells at days 7, 10 and 14 of culture determined by immunoblotting. **e**, Immunoprecipitation of c-Jun and JunB complexes demonstrates that HA-28z CAR T cells contain more c-Jun heterodimers, as well as JunB–IRF4, JunB–BATF and JunB–BATF3 heterodimers, than CD19-28z CAR T cells. **f**, Correlation network of exhaustion-related transcription factors in naive-derived CD4$^+$ GD2-28z CAR T cells using single-cell RNA-seq analysis. For gel source data, see Supplementary Fig. 1.

state in HA-28z CAR T cells regardless of the starting subset (Fig. 1i). HA-28z CAR T cells demonstrated increased chromatin accessibility near exhaustion-associated genes such as *CTLA4*, and decreased accessibility near memory-associated genes such as *IL7R* (Fig. 1j). Together, these data suggest that tonically signalling CAR T cells are a valid model for the study of human T cell exhaustion.

Epigenetic and transcriptional dysregulation of AP-1

Using ChromVAR[24] and transcription factor motif enrichment analysis to identify transcriptional programs associated with the epigenetic changes observed, we discovered that the AP-1–bZIP and bZIP–IRF binding motifs were the most significantly enriched in exhausted CAR T cells (Fig. 2a, b, Extended Data Fig. 4c, d), with strong enrichment of NF-κB, NFAT and RUNX transcription factor motifs in some clusters, reproducing epigenetic signatures of exhaustion observed in other models[18,20,25]. Paired RNA-seq analysis across three donors revealed increased bZIP and IRF mRNA in HA-28z versus CD19-28z CAR T cells, most significantly for *JUNB*, *FOSL1*, *BATF*, *BATF3*, *ATF3*, *ATF4* and *IRF4* (Fig. 2c, Extended Data Fig. 4e). We confirmed increased protein expression of JunB, IRF4 and BATF3, with higher relative levels of the BATF and IRF4 transcription factors than the canonical AP-1 factor c-Jun (Fig. 2d, Extended Data Fig. 4f). Transcription factors of the AP-1 family form homo- and heterodimers through interactions in the common bZIP domain that compete for binding at DNA elements containing core TGA-G/C-TCA consensus motifs and can complex with IRF transcription factors[7,9]. The classic AP-1 heterodimer c-Fos–c-Jun drives transcription of *IL2*, whereas complexes containing other AP-1 and IRF family members can antagonize c-Jun activity and/or drive immunoregulatory gene expression in T cells[7–10,26–28]. Co-immunoprecipitation analysis demonstrated increased levels of complexed JunB, BATF, BATF3 and IRF4 in HA-28z CAR T cells (Fig. 2e) and single-cell RNA-seq analysis of CD19-28z and GD2-28z CAR T cells confirmed that the bZIP family members *JUN*, *JUNB*, *JUND* and *ATF4* were among the most differentially expressed and broadly connected in exhausted GD2-28z CAR T cell networks (Fig. 2f, Extended Data Figs. 2, 4g). We observed a similar pattern of AP-1 and BATF/IRF4 imbalance in a single-cell gene expression dataset from patients with metastatic melanoma undergoing treatment with immune checkpoint blockade[29] (Extended Data Fig. 4h).

c-Jun overexpression prevents CAR T cell exhaustion

We hypothesized that T cell dysfunction in exhausted cells might be due to a relative deficiency in c-Jun–c-Fos AP-1 heterodimers. Indeed, HA-28z CAR T cells overexpressing AP-1 demonstrated increased production of IL-2, which required c-Jun but not c-Fos (Extended Data Fig. 4i-m), whereas no benefit was observed in CD19-28z CAR T cells.

To further investigate c-Jun overexpression in exhausted T cells, we created JUN-P2A-CAR bi-cistronic vectors (Fig. 3a, b) and demonstrated enhanced c-Jun N-terminal phosphorylation (JNP) only in JUN-HA-28z (Fig. 3c), consistent with JNK kinase activation via the HA-28z-associated tonic signal[30]. Antigen-stimulated JUN-HA-28z CAR T cells demonstrated remarkably increased production of IL-2 and IFNγ, although no significant differences were observed in JUN-CD19-28z CAR T cells (Fig. 3d, e, Extended Data Fig. 5b, c). We also observed enhanced functional activity of JUN-HA-28z CAR T cells at the single-cell level in both CD4$^+$ and CD8$^+$ CAR T cells, and c-Jun overexpression increased the frequency of stem-cell-memory and central-memory versus effector and effector-memory subsets in CD4$^+$ and CD8$^+$ populations of exhausted CAR T cells, but not in healthy CAR T cells (Fig. 3f, Extended

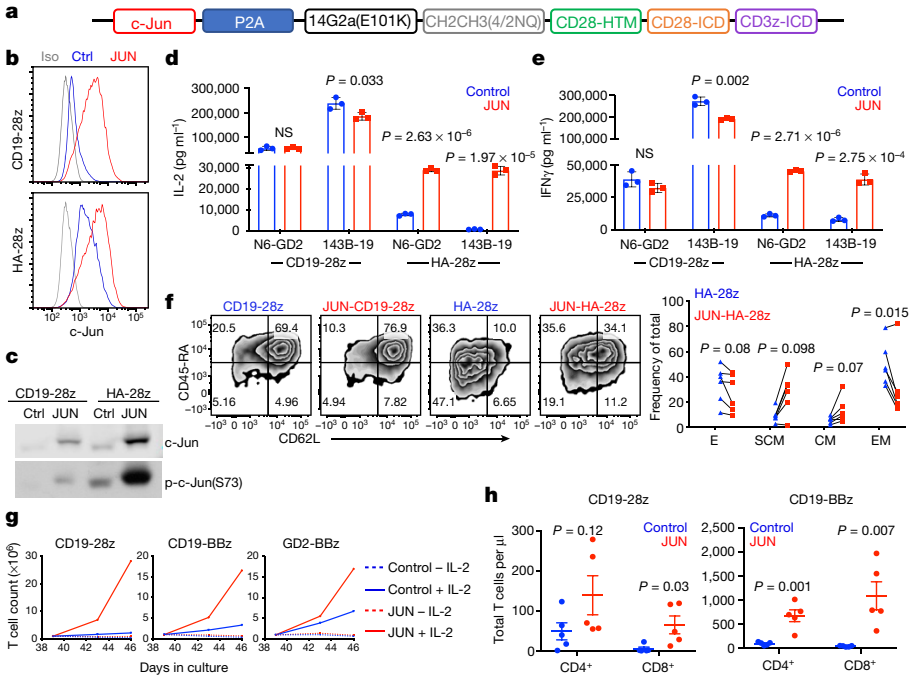

Fig. 3 | c-Jun overexpression enhances the function of exhausted CAR T cells. **a**, JUN-P2A-HA-CAR expression vector. HTM, hinge/transmembrane; ICD, intracellular domain. **b**, Intracellular c-Jun expression in control (Ctrl) and JUN CAR T cells at day 10 by flow cytometry. Grey denotes isotype control. **c**, Immunoblot for total c-Jun and phosphorylated c-Jun (p-c-Jun(S73)) in control (Ctrl) and JUN CAR T cells at day 10. **d**, **e**, IL-2 (**d**) and IFNγ (**e**) production after 24-h co-culture of control or JUN CD19-28z and HA-28z CAR T cells in response to antigen-positive tumour cells. Data are mean ± s.d. of triplicate wells. *P* values determined by unpaired two-tailed *t*-tests. One representative donor. Fold change across $n = 8$ donors in Extended Data Fig. 5. **f**, Left, flow cytometry showing representative expression of CD45RA and CD62L in control and JUN CAR T cells at day 10. Right, relative frequency of effector (E; CD45RA$^+$CD62L$^-$), stem-cell memory (SCM; CD45RA$^+$CD62L$^+$), central memory (CM; CD45RA$^-$CD62L$^+$), and effector memory (EM; CD45RA$^-$CD62L$^-$) in CD8$^+$ control or JUN-HA-28z CAR T cells ($n = 6$ donors from independent experiments). Lines indicate paired samples from the same donor. *P* values determined by paired two-tailed *t*-tests. **g**, On day 39, 1×10^6 viable T cells from Extended Data Fig. 5f were re-plated and cultured for 7 days with or without IL-2. **h**, Control or JUN CD19-28z or CD19-BBz CAR T cells from **g** were cryopreserved on day 10 and later thawed, rested overnight in IL-2 and 5×10^6 cells were then injected intravenously into healthy NSG mice. On day 25 after infusion, peripheral blood T cells were quantified by flow cytometry. Data are mean ± s.e.m. of $n = 5$ mice per group. *P* values determined by unpaired two-tailed *t*-tests.

Data Fig. 5d, e). Together, the data are consistent with a model in which c-Jun overexpression is functionally more significant in exhausted T cells, which express higher levels of immunomodulatory bZIP and IRF transcription factors.

Overexpression of c-Jun also enhanced long-term proliferative capacity, which is associated with anti-tumour effects in solid tumours[31], in CAR T cells without tonic signalling (CD19-28z, CD19-BBz) (Extended Data Fig. 5f). Enhanced proliferation remained IL-2-dependent, as expansion immediately ceased after IL-2 withdrawal (Fig. 3g, Extended Data Fig. 5g). Expanding CD8$^+$ JUN-CD19-28z CAR T cells displayed diminished exhaustion markers and an increased frequency of cells bearing the stem-cell memory phenotype compared with control CD19-28z CAR T cells (Extended Data Fig. 5h–j). c-Jun overexpression also increased homeostatic expansion of both CD19-28z and CD19-BBz CAR T cells in tumour-free NSG (NOD–SCID *Il2rg*-null) mice (Fig. 3h), which led to accelerated GVHD in the JUN-CD19-BBz CAR-T-cell-treated mice. Together, the data demonstrate that c-Jun overexpression mitigates T cell exhaustion in numerous CARs tested, including those incorporating CD28 or 4-1BB costimulatory domains, and regardless of whether exhaustion is driven by long-term expansion or tonic signalling.

Molecular mechanisms of c-Jun in exhaustion

To explore the mechanism by which c-Jun overexpression prevents T cell dysfunction, we compared ATAC-seq and RNA-seq results of HA-28z and JUN-HA-28z CAR T cells. Overexpression of c-Jun did not change the epigenetic profile but substantially modulated the transcriptome, with 319 genes differentially expressed in JUN and control HA-28z CAR T cells (Extended Data Fig. 6a–c), including reduced expression of exhaustion-associated genes and increased expression of memory genes. Using DAVID, we confirmed that genes changed by c-Jun are highly enriched for AP-1 family binding sites (Extended Data Fig. 6d), which suggests that gene expression changes were mediated by AP-1 family transcription factors.

We postulated that c-Jun overexpression could rescue exhausted T cells by direct transcriptional activation of AP-1 target genes and/or by indirectly disrupting immunoregulatory AP-1–IRF transcriptional complexes[7,9] that drive exhaustion-associated gene expression (AP-1i) (Extended Data Fig. 6e). To test these non-mutually-exclusive hypotheses, we first evaluated a panel of c-Jun mutants predicted to be deficient in transcriptional activation (JUN-AA, JUN-Δδ, JUN-ΔTAD), DNA binding (JUN-Δbasic) or dimerization (JUN-ΔLeu, JUN-ΔbZIP)[32–34] (Fig. 4a, Extended Data Fig. 6f). JUN-AA and JUN-Δδ both equivalently increased IL-2 and IFNγ production compared to wild-type c-Jun in HA-28z CAR T cells (Fig. 4b), whereas JUN-ΔTAD demonstrated partial rescue in IL-2 production. Conversely, C-terminal mutants (JUN-Δbasic, JUN-ΔLeu and JUN-ΔbZIP), which were unable to bind chromatin (Extended Data Fig. 6g), did not rescue cytokine production in exhausted HA-28z CAR T cells (Fig. 4b). Furthermore, c-Jun overexpression substantially decreased levels of AP-1i, as evidenced by diminished mRNA levels (Extended Data Fig. 6h), reduced total and chromatin-bound JunB, BATF and BATF3 proteins, and reduced JunB–BATF complexes (Extended Data

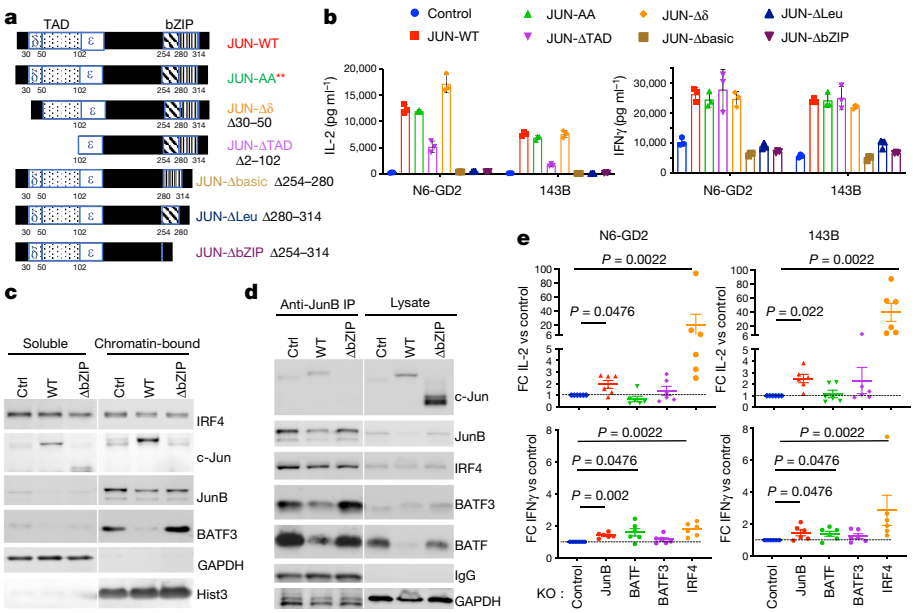

Fig. 4 | c-Jun functional rescue of exhaustion requires bZIP dimerization but is independent of transactivation. a, Schematic of c-Jun protein showing N-terminal transactivation domain (TAD) and C-terminal bZIP domain deletion mutants. Red asterisks denote JNP sites at Ser63 and Ser73 mutated to alanine in JUN-AA. **b**, IL-2 (left) and IFNγ (right) production by control or JUN-HA-28z CAR T cells expressing the indicated c-Jun variant after 24-h stimulation with Nalm6-GD2 (N6-GD2) or 143B target cells. Data are mean ± s.d. of triplicate wells; representative of three independent experiments. **c**, Immunoblot of indicated AP-1 and IRF proteins in control, JUN-WT or JUN-ΔbZIP HA-28z CAR T cells in soluble or chromatin-bound lysis fractions. **d**, Immunoblot of indicated AP-1 and IRF proteins in control, JUN-WT or JUN-ΔbZIP HA-28z CAR T cells in total lysate (right) or after JunB immunoprecipitation (IP, left). **e**, Fold change (FC) in IL-2 (top) and IFNγ (bottom) production in AP-1 or IRF4 CRISPR-knockout (KO) HA-28z CAR T cells after 24-h stimulation with Nalm6-GD2 or 143B target cells. Fold change in cytokine production is normalized to control HA-28z CAR T cells. Data are mean ± s.e.m. of $n = 6$ independent experiments. *P* values determined using nonparametric Mann–Whitney *U* tests.

Fig. 7a–c). Importantly, c-Jun-mediated displacement of JunB, BATF and BATF3 from chromatin and reduced JunB–BATF complexes were dependent on the ability of c-Jun to partner with AP-1 family members (Fig. 4c, d). Consistent with this, c-Jun and IRF4 chromatin immunoprecipitation followed by high-throughput sequencing (ChIP–seq) analysis identified no novel c-Jun-binding sites after c-Jun overexpression. Instead, the vast majority of sites bound by c-Jun are also bound by IRF4 (and probably BATF), consistent with c-Jun overexpression increasing binding almost exclusively at AP-1–IRF composite elements, including near exhaustion-associated genes regulated by IRF4, and genes associated with increased T cell proliferation and functional activation (Extended Data Fig. 7d–h). Finally, JunB-knockout, BATF-knockout and especially IRF4-knockout significantly increased IL-2 and IFNγ production in HA-28z CAR T cells (Fig. 4e, Extended Data Fig. 7i, j). Time-course experiments using a drug regulatable expression model of c-Jun revealed that full rescue required c-Jun overexpression during both T cell expansion and antigen stimulation (Extended Data Fig. 8), consistent with a model in which c-Jun overexpression both modulates molecular reprogramming during the development of exhaustion and augments responses during acute stimulation downstream of antigen encounter. Together, the data are consistent with a model in which an overabundance of AP-1–IRF complexes drives the exhaustion transcriptional program and c-Jun overexpression prevents exhaustion by decreasing and/or displacing AP-1i complexes from chromatin.

JUN CAR T cells enhance anti-tumour activity in vivo

Using a Nalm6-GD2$^+$ leukaemia model, we confirmed functional superiority of JUN-HA-28z CAR T cells in vivo (Fig. 5a–c), which required c-Jun dimerization but not transactivation (Extended Data Fig. 7k, l). In an in vitro model of limiting antigen dilution, JUN-HA-28z CAR T cells produced greater maximal IL-2 and IFNγ and manifested a lower threshold for antigen-induced IL-2 secretion (Fig. 5d, e). Limiting target antigen expression is increasingly recognized to limit CAR functionality as observed after treatment of CD22-BBz-CAR T cells in patients with relapsed or refractory leukaemia[12,13,35]. We therefore assessed whether c-Jun overexpression could enhance the capacity to target antigen-low tumour cells. In response to CD22^{low} leukaemia, JUN-CD22-BBz CAR T cells exhibited increased cytokine production in vitro (Fig. 5f–h) and markedly increased anti-tumour activity in vivo (Fig. 5i–l) compared with control CD22-BBz CAR T cells. Similar results were observed in a CD19^{low} Nalm6 leukaemia model (Extended Data Fig. 9a–f).

c-Jun decreases hypofunction within solid tumours

c-Jun overexpression also enhanced the functionality of CARs targeting solid tumours. JUN-Her2-BBz CAR T cells prevented 143B osteosarcoma tumour growth in vivo, markedly improved long-term survival, and greatly increased T cell expansion (Extended Data Fig. 9g–i). Similar results were observed when comparing GD2-BBz and JUN-GD2-BBz CAR T cells against 143B (Extended Data Fig. 9j–n). c-Jun overexpression increased the frequency of total and CAR$^+$ Her2-BBz T cells within tumours (Fig. 6a, b), reduced expression of exhaustion markers PD-1 and CD39 (Fig. 6c), and substantially increased cytokine production after ex vivo re-stimulation (Fig. 6d, e, Extended Data Fig. 10a–c). Single-cell RNA-seq of purified tumour infiltrating JUN-Her2-BBz CAR T cells demonstrated increased frequency of cells within the G2/M and S phases of the cell cycle (Fig. 6f), a more activated transcriptional program (as measured by *IL2RA* and *CD38*), and downregulation of numerous exhaustion-associated genes (*PDCD1*, *BTLA*, *TIGIT*, *CD200*, *ENTPD1* and *NR4A2*) (Fig. 6g and Extended Data Fig. 10d–g). Finally, a small cluster of T cells characterized by high *IL7R* expression (*IL7R*, *KLF2*, *CD27*, *TCF7* and *SELL*) was preserved in tumours treated with JUN CAR T cells but not those receiving control Her2-BBz CAR T cells (Extended Data Fig. 10g), consistent with c-Jun-induced maintenance of a memory-like population capable of self-renewal.

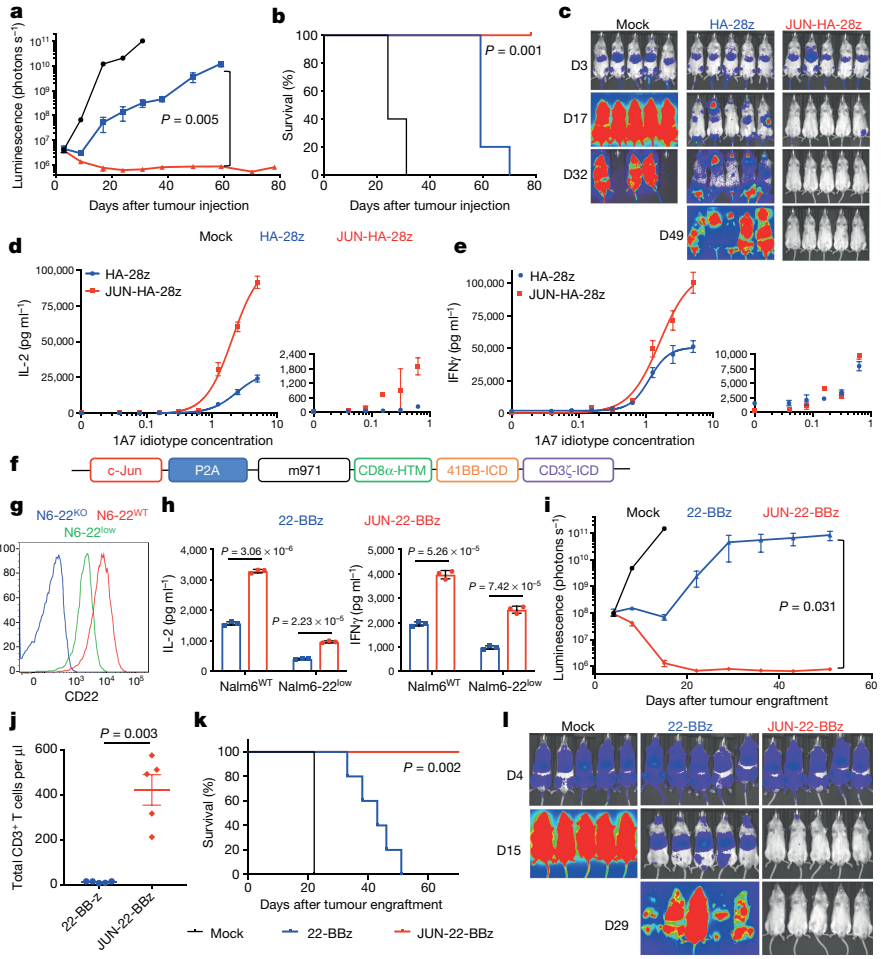

Fig. 5 | JUN-modified CAR T cells increase in vivo activity against leukaemia and enhance T cell function under suboptimal stimulation. a–**c**, NSG mice were injected intravenously with 1×10^6 Nalm6-GD2 leukaemia cells, and then 3×10^6 mock, HA-28z or JUN-HA-28z CAR$^+$ T cells were given intravenously on day 3. **a**, **c**, Tumour progression was monitored using bioluminescent imaging. Scales are normalized for all time points. D, day. **b**, JUN-HA-28z CAR T cells induced long-term tumour-free survival. Data are mean ± s.e.m. of $n = 5$ mice per group. Reproducible in three independent experiments; however, in some experiments, long-term survival was diminished owing to outgrowth of GD2(−) Nalm6 clones. **d**, **e**, IL-2 (**d**) and IFNγ (**e**) production after 24 h stimulation of control or JUN HA-28z CAR T cells with immobilized 1A7 anti-CAR idiotype antibody. Each curve was fit with nonlinear dose response kinetics to determine half-maximal effective concentration (EC_{50}) values. Smaller graphs (right) highlight antibody concentrations less than 1 μg ml^{-1}. Data are mean ± s.d. of triplicate wells; representative of two independent experiments. **f**, JUN-CD22-BBz retroviral vector. **g**, CD22 surface expression on Nalm6 wild-type (N6-22^{WT}), Nalm6-CD22-knockout (N6-22^{KO}) and Nalm6-22^{KO} plus CD22^{low} (N6-22^{low}) cells. **h**, IL-2 (left) and IFNγ (right) release after co-culture of Nalm6 and Nalm6-22^{low} cells with control or JUN-CD22-BBz CAR T cells. Data are mean ± s.d. of triplicate wells; representative of three independent experiments. **i**–**l**, NSG mice were inoculated with 1×10^6 Nalm6-22^{low} leukaemia cells intravenously. On day 4, 3×10^6 mock, control or JUN-CD22-BBz CAR$^+$ T cells were transferred intravenously. **i**, **l**, Tumour growth was monitored by bioluminescent imaging. **j**, Mice receiving JUN-CD22-BBz CAR T cells display increased peripheral blood T cells on day 23. **k**, Long-term survival of CAR-treated mice. Data in **i** and **j** are mean ± s.e.m. of $n = 5$ mice per group; representative of two independent experiments. Unless otherwise noted, *P* values determined by unpaired two-tailed *t*-tests. Survival curves were compared using the log-rank Mantel–Cox test.

Discussion

Several lines of evidence implicate exhaustion in limiting the potency of CAR T cells[6,11,16,17]. Using a tonically signalling CAR that can induce the hallmark features of exhaustion in a controlled in vitro culture system, we identified AP-1-related bZIP–IRF families as major factors that drive exhaustion-associated gene expression. We tested the hypothesis that exhaustion-associated dysfunction results from increased levels of AP-1–IRF complexes leading to a functional deficiency in activating AP-1 Fos/Jun heterodimers. Consistent with this model, c-Jun overexpression prevented phenotypic and functional hallmarks of exhaustion and improved anti-tumour control in five tumour models, including the clinically relevant GD2-BBz and Her2-BBz CAR T cells and CD19 CAR T cells subjected to prolonged ex vivo expansion. JUN CAR T cells also demonstrated increased potency when encountering tumour cells with low antigen density.

Mechanistically, c-Jun overexpression could work by directly enhancing c-Jun-mediated transcriptional activation of genes such as *IL2*, and/or indirectly by disrupting or displacing AP-1i. Substantial orthogonal data are consistent with the indirect displacement model. First, the inability of Fos overexpression to enhance function is consistent with the displacement model, as Fos has not been described to heterodimerize with BATF proteins. Second, c-Jun mutant experiments demonstrated a crucial role for dimerization but not transactivation in the biology observed. Third, we observed a reduction in total and chromatin-bound JunB, BATF and BATF3 after c-Jun overexpression, and could reproduce functional enhancement of exhausted T cells after knockout of *IRF4* and *JUNB*. An indirect model in which c-Jun blocks access of AP-1i complexes to enhancer regions is also consistent with the previous finding that BACH2 protects from terminal effector differentiation by blocking AP-1 sites[36] as terminal effector differentiation is a hallmark of exhaustion in

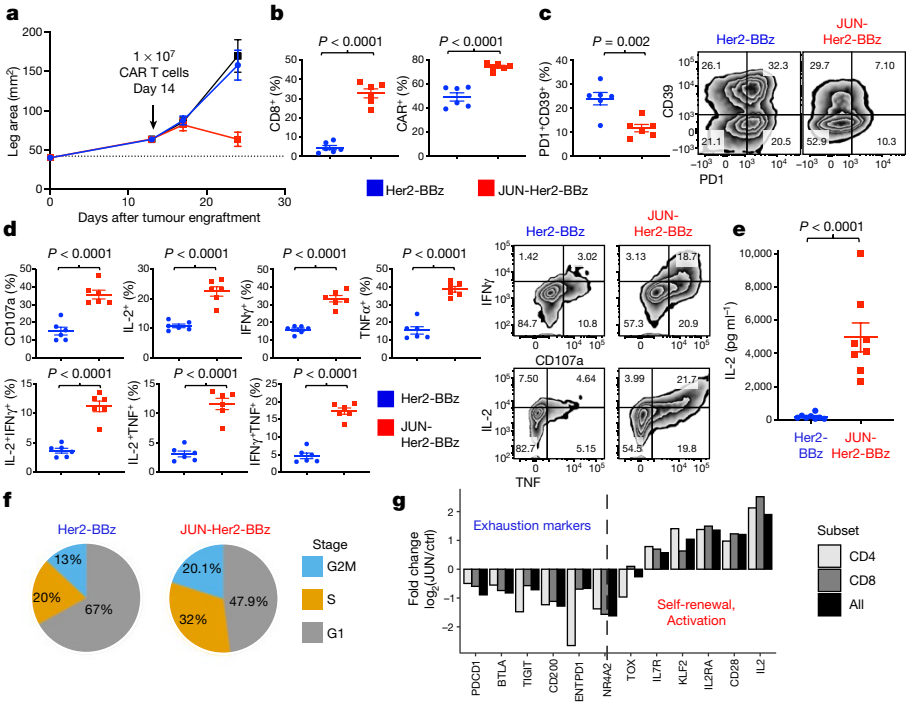

Fig. 6 | c-Jun overexpression enhances CAR T cell efficacy and decreases hypofunction within solid tumours. NSG mice were inoculated with 1×10^6 143B osteosarcoma cells via intramuscular injection, and then 1×10^7 mock, Her2-BBz or JUN-Her2-BBz CAR T cells were given intravenously on day 14. **a**, Tumour growth (monitored by caliper measurements). **b**–**g**, On day 28, mice were euthanized and tumour tissue was collected and mechanically dissociated. Single-cell suspensions were labelled for analysis by flow cytometry (**b**, **c**), re-stimulated with Nalm6-Her2$^+$ target cells and analysed for intracellular cytokine production (**d**), or sorted by FACS to isolate live, human CD45$^+$ tumour-infiltrating lymphocytes (TILs) (**e**–**g**). **b**, Left, CD8$^+$ cells as a proportion of total live tumour cells. Right, CAR$^+$ cells as a proportion of total live CD8$^+$ cells. **c**, PD-1$^+$CD39$^+$ cells as a frequency of total live CD8$^+$ (left) with representative contour plots (right). **d**, Frequency of indicated cytokine- or CD107a-producing cells after 5-h re-stimulation with Nalm6-Her2$^+$ target cells. Gated on total, live CD8$^+$ T cells (left) with representative contour plots (right). **e**, IL-2 secretion after 24-h re-stimulation of sorted CD45$^+$ TILs with Nalm6-Her2$^+$ target cells. Data in **a**–**e** are mean ± s.e.m. of $n = 6$–8 mice per group. Unless otherwise noted, P values determined by unpaired two-tailed t-tests. **f**, Relative frequency of sorted CD45$^+$ TILs in each phase of the cell cycle as determined by single-cell RNA-seq. **g**, The $\log_2$-transformed fold change in JUN compared with control Her2-BBz CAR T cells for the indicated transcripts.

our model and is prevented by c-Jun overexpression. Another related hypothesis suggests that exhaustion results from partner-less NFAT in the absence of AP-1[37] and several recent publications implicated the NFAT-driven transcription factors NR4A[38,39] and TOX[40–42] in T cell exhaustion. Overexpression of NR4A1 was shown to displace chromatin-bound c-Jun[38], suggesting that competition with NR4A family members might also contribute to the effects described here. Future studies are warranted to understand the functional overlap of NFAT, TOX and NR4A in c-Jun-overexpressing CAR T cells.

The impressive effects of c-Jun overexpression in several preclinical tumour models raise the prospect of clinical testing of JUN CAR T cells. c-Jun is the cellular homologue of the viral oncogene v-Jun[43], and c-Jun expression has been described in cancer[44,45]. However, c-Jun has not been implicated as an oncogene in mature T cells, which appear to be generally resistant to transformation, and we see no evidence for transformation in these studies. *Ras*-mediated transformation in rodent models requires JNP[46], therefore, the JUN-AA mutant, which equally rescues CAR T cell function, could be implemented to mitigate theoretical oncogenic risk. Future work is necessary to determine whether c-Jun overexpression might enhance the risk of other toxicities, including on-target and off-target effects.

In summary, our findings highlight the power of a deconstructed model of human T cell exhaustion to interrogate the biology of this complex phenomenon. Using this approach, we discovered a fundamental role for the AP-1–bZIP family in human T cell exhaustion and demonstrate that overexpression of c-Jun renders CAR T cells resistant to exhaustion, enhances their ability to control tumour growth in vivo, and improves the recognition of antigen-low targets, thus addressing major barriers to progress with this class of therapeutic agents.

Online content

Any methods, additional references, Nature Research reporting summaries, source data, extended data, supplementary information, acknowledgements, peer review information; details of author contributions and competing interests; and statements of data and code availability are available at https://doi.org/10.1038/s41586-019-1805-z.

1. Maude, S. L. et al. Tisagenlecleucel in children and young adults with b-cell lymphoblastic leukemia. *N. Engl. J. Med.* **378**, 439–448 (2018).
2. Neelapu, S. S. et al. Axicabtagene ciloleucel CAR T-cell therapy in refractory large B-cell lymphoma. *N. Engl. J. Med.* **377**, 2531–2544 (2017).
3. June, C. H., O'Connor, R. S., Kawalekar, O. U., Ghassemi, S. & Milone, M. C. CAR T cell immunotherapy for human cancer. *Science* **359**, 1361–1365 (2018).
4. Wherry, E. J. et al. Molecular signature of CD8$^+$ T cell exhaustion during chronic viral infection. *Immunity* **27**, 670–684 (2007).
5. Wherry, E. J. & Kurachi, M. Molecular and cellular insights into T cell exhaustion. *Nat. Rev. Immunol.* **15**, 486–499 (2015).
6. Long, A. H. et al. 4-1BB costimulation ameliorates T cell exhaustion induced by tonic signaling of chimeric antigen receptors. *Nat. Med.* **21**, 581–590 (2015).
7. Man, K. et al. Transcription factor IRF4 promotes CD8$^+$ T cell exhaustion and limits the development of memory-like T cells during chronic infection. *Immunity* **47**, 1129–1141 (2017).
8. Li, P. et al. BATF-JUN is critical for IRF4-mediated transcription in T cells. *Nature* **490**, 543–546 (2012).
9. Murphy, T. L., Tussiwand, R. & Murphy, K. M. Specificity through cooperation: BATF-IRF interactions control immune-regulatory networks. *Nat. Rev. Immunol.* **13**, 499–509 (2013).

10. Quigley, M. et al. Transcriptional analysis of HIV-specific CD8$^+$ T cells shows that PD-1 inhibits T cell function by upregulating BATF. *Nat. Med.* **16**, 1147–1151 (2010).
11. Fraietta, J. A. et al. Determinants of response and resistance to CD19 chimeric antigen receptor (CAR) T cell therapy of chronic lymphocytic leukemia. *Nat. Med.* **24**, 563–571 (2018).
12. Walker, A. J. et al. Tumor antigen and receptor densities regulate efficacy of a chimeric antigen receptor targeting anaplastic lymphoma kinase. *Mol. Ther.* **25**, 2189–2201 (2017).
13. Fry, T. J. et al. CD22-targeted CAR T cells induce remission in B-ALL that is naive or resistant to CD19-targeted CAR immunotherapy. *Nat. Med.* **24**, 20–28 (2018).
14. Hegde, M., Moll, A. J., Byrd, T. T., Louis, C. U. & Ahmed, N. Cellular immunotherapy for pediatric solid tumors. *Cytotherapy* **17**, 3–17 (2015).
15. Long, A. H. et al. Reduction of MDSCs with all-trans retinoic acid improves CAR therapy efficacy for sarcomas. *Cancer Immunol. Res.* **4**, 869–880 (2016).
16. Eyquem, J. et al. Targeting a CAR to the TRAC locus with CRISPR/Cas9 enhances tumour rejection. *Nature* **543**, 113–117 (2017).
17. Fraietta, J. A. et al. Disruption of TET2 promotes the therapeutic efficacy of CD19-targeted T cells. *Nature* **558**, 307–312 (2018).
18. Sen, D. R. et al. The epigenetic landscape of T cell exhaustion. *Science* **354**, 1165–1169 (2016).
19. Bengsch, B. et al. Epigenomic-guided mass cytometry profiling reveals disease-specific features of exhausted CD8 T cells. *Immunity* **48**, 1029–1045 (2018).
20. Pauken, K. E. et al. Epigenetic stability of exhausted T cells limits durability of reinvigoration by PD-1 blockade. *Science* **354**, 1160–1165 (2016).
21. Heczey, A. et al. CAR T cells administered in combination with lymphodepletion and PD-1 Inhibition to patients with neuroblastoma. *Mol. Ther.* **25**, 2214–2224 (2017).
22. Horwacik, I. et al. Structural basis of GD2 ganglioside and mimetic peptide recognition by 14G2a antibody. *Mol. Cell. Proteomics* **14**, 2577–2590 (2015).
23. Buenrostro, J. D., Giresi, P. G., Zaba, L. C., Chang, H. Y. & Greenleaf, W. J. Transposition of native chromatin for fast and sensitive epigenomic profiling of open chromatin, DNA-binding proteins and nucleosome position. *Nat. Methods* **10**, 1213–1218 (2013).
24. Schep, A. N., Wu, B., Buenrostro, J. D. & Greenleaf, W. J. chromVAR: inferring transcription-factor-associated accessibility from single-cell epigenomic data. *Nat. Methods* **14**, 975–978 (2017).
25. Philip, M. et al. Chromatin states define tumour-specific T cell dysfunction and reprogramming. *Nature* **545**, 452–456 (2017).
26. Meixner, A., Karreth, F., Kenner, L. & Wagner, E. F. JunD regulates lymphocyte proliferation and T helper cell cytokine expression. *EMBO J.* **23**, 1325–1335 (2004).
27. Chiu, R., Angel, P. & Karin, M. Jun-B differs in its biological properties from, and is a negative regulator of, c-Jun. *Cell* **59**, 979–986 (1989).
28. Echlin, D. R., Tae, H. J., Mitin, N. & Taparowsky, E. J. B-ATF functions as a negative regulator of AP-1 mediated transcription and blocks cellular transformation by Ras and Fos. *Oncogene* **19**, 1752–1763 (2000).
29. Sade-Feldman, M. et al. Defining T cell states associated with response to checkpoint immunotherapy in melanoma. *Cell* **175**, 998–1013 (2018).
30. Dérijard, B. et al. JNK1: a protein kinase stimulated by UV light and Ha-Ras that binds and phosphorylates the c-Jun activation domain. *Cell* **76**, 1025–1037 (1994).
31. D'Angelo, S. P. et al. Antitumor activity associated with prolonged persistence of adoptively transferred NY-ESO-1 ^{c259}T cells in synovial sarcoma. *Cancer Discov.* **8**, 944–957 (2018).
32. Adler, V., Franklin, C. C. & Kraft, A. S. Phorbol esters stimulate the phosphorylation of c-Jun but not v-Jun: regulation by the N-terminal delta domain. *Proc. Natl Acad. Sci. USA* **89**, 5341–5345 (1992).
33. Bannister, A. J., Oehler, T., Wilhelm, D., Angel, P. & Kouzarides, T. Stimulation of c-Jun activity by CBP: c-Jun residues Ser63/73 are required for CBP induced stimulation *in vivo* and CBP binding *in vitro*. *Oncogene* **11**, 2509–2514 (1995).
34. Weiss, C. et al. JNK phosphorylation relieves HDAC3-dependent suppression of the transcriptional activity of c-Jun. *EMBO J.* **22**, 3686–3695 (2003).
35. Majzner, R. G. & Mackall, C. L. Tumor antigen escape from CAR T-cell therapy. *Cancer Discov.* **8**, 1219–1226 (2018).
36. Roychoudhuri, R. et al. BACH2 regulates CD8$^+$ T cell differentiation by controlling access of AP-1 factors to enhancers. *Nat. Immunol.* **17**, 851–860 (2016).
37. Martinez, G. J. et al. The transcription factor NFAT promotes exhaustion of activated CD8$^+$ T cells. *Immunity* **42**, 265–278 (2015).
38. Liu, X. et al. Genome-wide analysis identifies NR4A1 as a key mediator of T cell dysfunction. *Nature* **567**, 525–529 (2019).
39. Chen, J. et al. NR4A transcription factors limit CAR T cell function in solid tumours. *Nature* **567**, 530–534 (2019).
40. Seo, H. et al. TOX and TOX2 transcription factors cooperate with NR4A transcription factors to impose CD8$^+$ T cell exhaustion. *Proc. Natl Acad. Sci. USA* **116**, 12410–12415 (2019).
41. Alfei, F. et al. TOX reinforces the phenotype and longevity of exhausted T cells in chronic viral infection. *Nature* **571**, 265–269 (2019).
42. Khan, O. et al. TOX transcriptionally and epigenetically programs CD8$^+$ T cell exhaustion. *Nature* **571**, 211–218 (2019).
43. Bohmann, D. et al. Human proto-oncogene c-jun encodes a DNA binding protein with structural and functional properties of transcription factor AP-1. *Science* **238**, 1386–1392 (1987).
44. Mariani, O. et al. JUN oncogene amplification and overexpression block adipocytic differentiation in highly aggressive sarcomas. *Cancer Cell* **11**, 361–374 (2007).
45. Shaulian, E. AP-1–The Jun proteins: Oncogenes or tumor suppressors in disguise? *Cell. Signal.* **22**, 894–899 (2010).
46. Behrens, A., Jochum, W., Sibilia, M. & Wagner, E. F. Oncogenic transformation by ras and fos is mediated by c-Jun N-terminal phosphorylation. *Oncogene* **19**, 2657–2663 (2000).

Methods

Viral vector construction

MSGV retroviral vectors encoding the following CARs were previously described: CD19-28z, CD19-BBz, GD2-28z, GD2-BBz, Her2-BBz and CD22-BBz. To create the HA-28z CAR, a point mutation was introduced into the 14G2a scFv of the GD2-28z CAR plasmid to create the E101K mutation. The '4/2NQ' mutations[47] were introduced into the CH2CH3 domains of the IgG1 spacer region to diminish Fc receptor recognition for in vivo use of HA-28z CAR T cells.

Codon-optimized cDNAs encoding c-Jun (*JUN*), c-Fos (*FOS*), and truncated NGFR (tNGFR; *NGFR*) were synthesized by IDT and cloned into lentiviral expression vectors to create JUN-P2A-FOS, and JUN and FOS single expression vectors co-expressing tNGFR under the separate PGK promoter. JUN-P2A was then subcloned into the XhoI site of MSGV CAR vectors using the In-Fusion HD cloning kit (Takara) upstream of the CAR leader sequence to create JUN-P2A-CAR retroviral vectors. For JUN-AA, point mutations were introduced to convert Ser63 and Ser73 to Ala. The other JUN mutants were cloned to remove portions of the protein as described in Fig. 4. The *Escherichia coli* DHFR-destabilization domain (DD) sequence was inserted upstream of Jun to create JUN-DD fusion constructs. In some cases, GFP cDNA was subcloned upstream of the CAR to create GFP-P2A-CAR vector controls. For bi-cistronic CAR retroviral vectors, the HA-28z or Her2-28z CAR was cloned downstream of a codon-optimized CD19-28z CAR to create CD19-28z-P2A-HA-28z and CD19-28z-P2A-Her2-28z dual CAR expression vectors.

Viral vector production

Retroviral supernatant was produced in the 293GP packaging cell line as previously described[6]. In brief, 70% confluent 293GP 20-cm plates were co-transfected with 20 μg MSGV vector plasmid and 10 μg RD114 envelope plasmid DNA using Lipofectamine 2000. Medium was replaced at 24 and 48 h after transfection. The 48-h and 72-h viral supernatants were collected, centrifuged to remove cell debris, and frozen at −80 °C for future use. Third-generation, self-inactivating lentiviral supernatant was produced in the 293T packaging cell line. In brief, 70% confluent 293T 20-cm plates were co-transfected with 18 μg pELNS vector plasmid, and 18 μg pRSV-Rev, 18 μg pMDLg/pRRE (Gag/Pol) and 7 μg pMD2.G (VSVG envelope) packaging plasmid DNA using Lipofectamine 2000. Medium was replaced at 24 h after transfection. The 24-h and 48-h viral supernatants were collected, combined and concentrated by ultracentrifugation at 28,000 rpm for 2.5 h. Concentrated lentiviral stocks were frozen at −80 °C for future use.

T cell isolation

Healthy donor buffy coats were collected by and purchased from the Stanford Blood Center under an IRB-exempt protocol. Primary human T cells were isolated using the RosetteSep Human T cell Enrichment kit (Stem Cell Technologies) according to the manufacturer's protocol using Lymphoprep density gradient medium and SepMate-50 tubes. Isolated T cells were cryopreserved at 2×10^7 T cells per vial in CryoStor CS10 cryopreservation medium (Stem Cell Technologies).

CAR T cell production

Cryopreserved T cells were thawed and activated same day with Human T-Expander CD3/CD28 Dynabeads (Gibco) at 3:1 beads:cell ratio in T cell medium (AIMV supplemented with 5% fetal bovine serum (FBS), 10 mM HEPES, 2 mM GlutaMAX, 100 U ml^{-1} penicillin and 100 μg ml^{-1} streptomycin (Gibco)). Recombinant human IL-2 (Peprotech) was provided at 100 U ml^{-1}. T cells were transduced with retroviral vector on days 2 and 3 after activation and maintained at 0.5×10^6–1×10^6 cells per ml in T cell medium with IL-2. Unless otherwise indicated, CAR T cells were used for in vitro assays or transferred into mice on days 10–11 afteractivation.

Retroviral transduction

Non-tissue culture treated 12-well plates were coated overnight at 4 °C with 1 ml Retronectin (Takara) at 25 μg ml^{-1} in PBS. Plates were washed with PBS and blocked with 2% BSA for 15 min. Thawed retroviral supernatant was added at approximately 1 ml per well and centrifuged for 2 h at 32 °C at 3,200 rpm before the addition of cells.

CRISPR knockout

CRISPR–Cas9 gene knockout was performed by transient Cas9/gRNA (RNP) complex electroporation using the P3 Primary Cell 4D-Nucleofector X Kit S (Lonza). On day 4 of culture, HA-28z CAR T cells were counted, pelleted and resuspended in P3 buffer at 1.5×10^6–2×10^6 cells per 20 μl reaction. 3.3ug Alt-R .Sp. Cas9 protein (IDT) and 40pmol chemically modified synthetic sgRNA (Synthego) (2:1 molar ratio gRNA:Cas9) per reaction was pre-complexed for 10 min at room temperature to create ribonucleoprotein complexes (RNP). A 20-μl cell suspension was mixed with RNP and electroporated using the EO-115 protocol in 16-well cuvette strips. Cells were recovered at 37 °C for 30 min in 200 μl T cell medium then expanded as described above. Knockdown efficiency was determined using TIDE and/or immunoblot. Control HA-28z CAR T cells were electroporated with a gRNA targeting the safe-harbour locus AAVS1. The following gRNA target sequences were used: AAVS1- GGGGCCACTAGGGACAGGAT, JUNB-ACTCCTGAAACCGAGC CTGG, BATF-TCACTGCTGTCGGAGCTGTG, BATF3-CGTCCTGCAGAG GAGCGTCG, and IRF4-CGGAGAGTTCGGCATGAGCG.

Cell lines

The Kelly neuroblastoma, EW8 Ewing's sarcoma, 143b and TC32 osteosarcoma cell lines were originally obtained from ATCC. In some cases, cell lines were stably transduced with GFP and firefly luciferase (GL). The $CD19^+CD22^+$ Nalm6-GL B-ALL cell line was provided by D. Barrett. Nalm6-GD2 was created by co-transducing Nalm6-GL with cDNAs for GD2 synthase and GD3 synthase. The Nalm6-Her2 cell line was created using lentiviral overexpression of Her2 cDNA. Single-cell clones were then chosen for high antigen expression. Nalm6-22-knockout ($Nalm6\text{-}22^{KO}$) and $Nalm6\text{-}22^{KO}$ plus $CD22^{low}$ ($N6\text{-}22^{low}$) have been previously described and were provided by T. Fry[13]. The $Nalm6\text{-}CD19^{low}$ cell lines were created by R. Majzner (manuscript in preparation). All cell lines were cultured in complete media (CM) (RPMI supplemented with 10% FBS, 10 mM HEPES, 2 mM GlutaMAX, 100 U ml^{-1} penicillin, and 100 μg ml^{-1} streptomycin (Gibco)). STR DNA profiling of all cell lines is conducted by Genetica Cell Line testing once per year. None of the cell lines used in this study is included in the commonly misidentified cell lines registry. Before using for in vivo experiments, cell lines were tested with MycoAlert detection kit (Lonza). All cell lines tested negative.

Flow cytometry

The anti-CD19 CAR idiotype antibody was provided by B. Jena and L. Cooper[48]. The 1A7 anti-14G2a idiotype antibody was obtained from NCI-Frederick. CD22 and Her2 CARs were detected using human CD22-Fc and Her2-Fc recombinant proteins (R&D). The idiotype antibodies and Fc-fusion proteins were conjugated in house with Dylight488 and/or 650 antibody labelling kits (Thermo Fisher). T cell surface phenotype was assessed using the following antibodies:

From BioLegend: CD4-APC-Cy7 (clone OKT4), CD8-PerCp-Cy5.5 (clone SK1), TIM-3-BV510 (clone F38-2E2), CD39-FITC or APC-Cy7 (clone A1), CD95-PE (clone DX2), CD3-PacBlue (clone HIT3a).

From eBioscience: PD-1-PE-Cy7 (clone eBio J105), LAG-3-PE (clone 3DS223H), CD45RO-PE-Cy7 (clone UCHL1), CD45-PerCp-Cy5.5 (clone HI30).

From BD: CD45RA-FITC or BV711 (clone HI100), CCR7-BV421 (clone 150503), CD122-BV510 (clone Mik-β3), CD62L-BV605 (clone DREG-56), CD4-BUV395 (clone SK3), CD8-BUV805 (clone SK1).

Cytokine production

Approximately 1×10^5 CAR$^+$ T cells and 1×10^5 tumour cells were cultured in 200 µl CM in 96-well flat bottom plates for 24 h. For idiotype stimulation, serial dilutions of 1A7 were crosslinked in 1× Coating Buffer (BioLegend) overnight at 4 °C on Nunc Maxisorp 96-well ELISA plates (Thermo Scientific). Wells were washed once with PBS and 1×10^5 CAR$^+$ T cells were plated in 200 µl CM and cultured for 24 h. Triplicate wells were plated for each condition. Culture supernatants were collected and analysed for IFNγ and IL-2 by ELISA (BioLegend).

Intracellular cytokine staining

For Intracellular cytokine staining analysis, CAR$^+$ T cells and target cells were plated at 1:1 effector:target ratio in CM containing 1× monensin (eBioscience) and 5 µl per test CD107a antibody (BV605, Clone H4A3, BioLegend) for 5–6 h. After incubation, intracellular cytokine staining was performed using the FoxP3 TF Staining Buffer Set (eBioscience) according to the manufacturer's instruction using the following antibodies from BioLegend: IL2-PECy7 Clone MQ1-17H12, IFNγ-APC/Cy7 Clone 4S.B3, and TNFα-BV711 Clone Mab11.

Incucyte lysis assay

Approximately 5×10^4 GFP$^+$ leukaemia cells were co-cultured with CAR T cells in 200 µl CM in 96-well flat bottom plates for up to 120 h. Triplicate wells were plated for each condition. Plates were imaged every 2–3 h using the IncuCyte ZOOM Live-Cell analysis system (Essen Bioscience). Four images per well at 10× zoom were collected at each time point. Total integrated GFP intensity per well was assessed as a quantitative measure of live, GFP$^+$ tumour cells. Values were normalized to the starting measurement and plotted over time. Effector:target ratios are indicated in the figure legends.

Immunoblotting and immunoprecipitations

Whole-cell protein lysates were obtained in non-denaturing buffer (150 mM NaCl, 50 mM Tris pH 8, 1% NP-10, 0.25% sodium deoxycholate). Protein concentrations were estimated by Bio-Rad colorimetric assay. Immunoblotting was performed by loading 20 µg of protein onto 11% PAGE gels followed by transfer to PVF membranes. Signals were detected by enhanced chemiluminescence (Pierce) or with the Odyssey imaging system. Representative blots are shown. The following primary antibodies used were purchased from Cell Signaling: c-Jun (60A8), P-c-Jun^{Ser73} (D47G9), JunB(C37F9), BATF(D7C5), IRF4(4964) and Histone-3(1B1B2). The BATF3 (AF7437) antibody was from R&D. Immunoprecipitations were performed in 100 µg of whole-cell protein lysates in 150 µl of nondenaturing buffer and 7.5 µg of agar-conjugated antibodies c-Jun (G4) or JunB (C11) (Santa Cruz Biotechnology). After overnight incubation at 4 °C, beads were washed three times with nondenaturing buffer, and proteins were eluted in Laemmli sample buffer, boiled and loaded onto PAGE gels. Detection of immunoprecipitated proteins was performed with above-mentioned reagents and antibodies.

Preparation of chromatin fractions

Separation of chromatin-bound from soluble proteins was performed as previously described[49] using cytoskeletal (CSK) buffer: 10 mM PIPES-KOH (pH 6.8), 100 mM NaCl, 300 mm sucrose, 3 mM $MgCl_2$, 0.5 mM PMSF, 0.1 mM glycerolphosphate, 50 mM NaF, 1 mM Na_3VO_4, containing 0.1% Nonidet P-40 and protease inhibitors 2 mM PMSF, 10 µg ml^{-1} leupeptin, 4 µg ml^{-1} aprotinin, and 4 µg ml^{-1} pepstatin. In brief, cell pellets were lysed for 10 min on ice followed by 5,000 rpm centrifugation at 4 °C for 5 min. The soluble fraction was collected and cleared by high-speed centrifugation, 13,000 rpm for 5 min. Protein concentration was determined by Bradford assays. Pellets containing chromatin-bound proteins were washed with CSK buffer and centrifuged at 5,000 rpm at 4 °C for 5 min. Chromatin-bound proteins were solubilized in 1× Laemmli Sample Buffer and boiled for 5 min. Equal volumes of chromatin and soluble fraction were loaded for each sample and analysed by immunoblotting.

ChIP and library preparation

Twenty-million CAR T cells were fixed with 1% formaldehyde for 10 min at room temperature. Cross-linking was quenched using 0.125 M glycine for 10 min before cells were washed twice with PBS. Cross-linked pellets were frozen with dry-ice ethanol and stored at −80 °C. Two biological replicates were collected for each cell culture. Chromatin immunoprecipitations were performed with exogenous spike-ins (ChIP-Rx) to allow for proper normalization, as previously described[50]. In brief, pellets were thawed on ice before cell membrane lysis in 5 ml LB1 by rotating for 10 min at 4 °C. Nuclei were pelleted at 1,350*g* for 5 min at 4 °C and lysed in 5 ml LB2 by rotating for 10 min at room temperature. Chromatin was pelleted at 1,350*g* for 5 min at 4 °C and resuspended in 1.5 ml LB3. Sonication was performed in a Bioruptor Plus until chromatin was 200–700 bp. Debris were pelleted and supernatants were collected and Triton X-100 was added to 1% final concentration. Ten per cent of the sample was collected as input controls. Anti-RF4 (Abcam Ab101168) or anti-c-Jun (Active Motif 39309) targeting antibodies were added at 5 µg per immunoprecipitate to sonicated lysate and rotated at 4 °C for 16–20 h.

Protein G Dynabeads (100 µl per immunoprecipitate) were washed three times with Block Solution (0.5% BSA in PBS). Antibody-bound chromatin was added to beads and rotated for 2–4 h at 4 °C. Bead-bound chromatin was washed five times with 1 ml RIPA wash buffer then once with 1 ml TE buffer with 500 mM NaCl. Beads were resuspended in 210 µl. Elution and chromatin was eluted at 65 °C for 15 min. Beads were magnetized and supernatant was removed to a fresh tube. Immunoprecipitated and input control chromatin was reverse cross-linked at 65 °C for 12–16 h.

Samples were diluted with 1 volume TE buffer. RNA was digested using 0.2 mg ml^{-1} RNase A (Qiagen 19101) for 2 h at 37 °C. $CaCl_2$ was added to 5.25 mM and samples were treated with 0.2 mg ml^{-1} proteinase K (Life Technologies EO0491) for 30 min at 55 °C. One volume phenol-chloroform-isoamyl alcohol was added and centrifuged 16,500*g* for 5 min to extract DNA, followed by a second extraction using one volume pure chloroform. Aqueous phase was removed and DNA was precipitated using two volumes ethanol and 0.3 M soduim acetate. DNA pellets were resuspended in EB elution buffer (Qiagen).

To prepare libraries for sequencing, DNA was end repaired using T4 polymerase (New England Biolabs M0203L), Klenow fragment (NEB M0210L), and T4 polynucleotide kinase (NEB M0201L) for 30 min at 20 °C. 3′ A-tailing was performed using Exo- Klenow fragment (NEB M0212L) for 30 min at 37 °C. Illumina TruSeq Pre-Indexed Adaptors (1 µM) or NEBNext Illumina Multiplex Oligo Adaptors (NEB E7335S) were ligated for 1 h at room temperature. Unligated adapters were separated by gel electrophoresis (2.5% agarose, 0.5× TBE) and ligated DNA was purified using a NucleoSpin Gel Clean-up Kit (Macherey-Nagel 740609.250). Ligated DNA was PCR amplified using TruSeq Primers 1.0 and 2.0 or NEBNext Multiplex Primers and purified using AMPure XP beads (Beckman Coulter A63881). Purified libraries were quantified using Agilent 2100 Bioanalyzer HS DNA and multiplexed in equimolar concentrations. Sequencing was performed using an Illumina NextSeq or HiSeq at 2 × 75 bp by Stanford Functional Genomics Facility.

Mice

Immunocompromised NOD-SCID-*Il2rg*$^{-/-}$ (NSG) mice were purchased from JAX and bred in-house. All mice were bred, housed and treated in ethical compliance with Stanford University IACUC (APLAC) approved protocols. Six-to-eight-week-old male or female mice were inoculated with either 1×10^6 Nalm6-GL leukaemia via intravenous or 0.5×10^6–1×10^6 143B osteosarcoma via intramuscular injections. All CAR T cells were injected intravenously. Time and treatment dose are indicated in the figure legends. Leukaemia progression was measured

by bioluminescent imaging using the IVIS imaging system. Values were analysed using Living Image software. Solid tumour progression was followed using caliper measurements of the injected leg area. Mice were humanely euthanized when an IACUC-approved end-point measurement reached 1.75 cm in either direction (for solid tumour) or when mice demonstrated signs of morbidity and/or hind-limb paralysis (leukaemia). Five-to-ten mice per group were treated in each experiment based on previous experience in these models, and each experiment was repeated two or three times as indicated. Mice were randomized to ensure equal pre-treatment tumour burden before CAR T cell treatment. In some experiments, researchers were blinded to treatment during tumour measurement.

Blood and tissue analysis

Peripheral blood sampling was conducted via retro-orbital blood collection under isoflurane anaesthesia at the indicated time points. Fifty microlitres of blood was labelled with CD45, CD3, CD4 and CD8, lysed using BD FACS Lysing Solution and quantified using CountBright Absolute Counting beads (Thermo Fisher) on a BD Fortessa flow cytometer. For ex vivo analysis of CAR TILs, 14 days after T cell treatment (day 28 after tumour engraftment), six mice per group were euthanized, solid tumour tissue was collected, mechanically dissociated using the gentleMACS dissociator (Miltenyi), and single-cell suspensions were either analysed by flow cytometry, re-plated with 3×10^5 Nalm6-Her2$^+$ target cells for ICS analysis, or labelled for sorting. Live, CD45$^+$ TILs were sorted from each tumour and re-stimulated at 1:1 effector:target ratio with Nalm6-Her2$^+$ target cells. Twenty-four-hour supernatant was analysed for IL-2 production by ELISA.

ATAC-seq

ATAC-seq library preparation was carried out as previously described[51]. In brief, 100,000 cells from each sample were sorted by FACS into CM, centrifuged at 500*g* at 4 °C, then resuspended in ATAC-seq resuspension buffer (RSB) (10 mM Tris-HCl, 10 mM NaCl, 3 mM $MgCl_2$) supplemented with 0.1% NP-40,0.1% Tween-20 and 0.01% digitonin. Samples were split into two replicates each before all subsequent steps. Samples were incubated on ice for 3 min, then washed out with 1 ml RSB supplemented with 0.1% Tween-20. Nuclei were pelleted at 500*g* for 10 min at 4 °C. The nuclei pellet was resuspended in 50 µl transposition mix (25 µl 2× TD buffer, 2.5 µl transposase (Illumina), 16.5 µl PBS, 0.5 µl 1% digitonin, 0.5 µl 10% Tween-20, 5 µl H_2O) and incubated at 37 °C for 30 min in a thermomixer with 1,000 rpm shaking. The reaction was cleaned up using the Qiagen MinElute PCR Purification Kit. Libraries were PCR-amplified using the NEBNext Hi-Fidelity PCR Master Mix and custom primers (IDT) as previously described[23]. Libraries were sufficiently amplified following 5 cycles of PCR, as indicated by qPCR fluorescence curves[23]. Libraries were purified with the Qiagen MinElute PCR Purification Kit and quantified with the KAPA Library Quantification Kit. Libraries were sequenced on the Illumina NextSeq at the Stanford Functional Genomics Facility with paired-end 75-bp reads. Adaptor sequences were trimmed using SeqPurge and aligned to hg19 genome using bowtie2. These reads were then filtered for mitochondrial reads, low mapping quality ($Q \geq 20$), and PCR duplicates using Picard tools. Then we converted the bam to a bed and got the Tn5 corrected insertion sites ('+' stranded + 4 bp, '−' stranded −5 bp). To identify peaks, we called peaks for each sample using MACS2 '–shift -75–extsize 150–nomodel–call-summits–nolambda–keep-dup all -p 0.00001' using the insertion beds. To get a union peak set, we (1) extended all summits to 500 bp; (2) merged all summit bed files; and (3) used bedtools cluster and selected the summit with the highest MACS2 score. This was then filtered by the ENCODE hg19 blacklist (https://www.encodeproject.org/annotations/ENCSR636HFF/), to remove peaks that extend beyond the ends of chromosomes. We then annotated these peaks using HOMER and computed the occurrence of a transcription factor motif using motifmatchr in R with chromVARMotifs HOMER set. To create sequencing tracks, we read the Tn5 corrected insertion sites into R and created a coverage pileup binned every 100 bp using rtracklayer. We then counted all insertions that fell within each peak to get a counts matrix (peak × samples). To determined differential peaks we first used peaks that were annotated as 'TSS' as control genes or 'housekeeping peaks' for DESeq2 and then computed differential peaks with this normalization. All clustering was performed using the regularized log transform values from DESeq2. Transcription factor motif deviation analysis was carried out using chromVAR as previously described[24]. Transcription factor motif enrichment were calculated using a hypergeometric test in R testing the representation of a motif (from motifmatchr above) in a subset of peaks vs all peaks.

Subset RNA-seq

For T cell subset-specific RNA-seq, T cells were isolated from healthy donor buffy coats as described above. Before activation, naive and central memory CD4$^+$ or CD8$^+$ subsets were isolated using a BD FACSAria cell sorter (Stem Cell FACS Core, Stanford University School of Medicine) using the following markers: naive (CD45RA$^+$CD45RO$^-$, CD62L$^+$, CCR7$^+$, CD95$^-$, and CD122$^-$), central memory (CD45RA$^-$CD45RO$^+$, CD62L$^+$, CCR7$^+$). Sorted starting populations were activated, transduced and cultured as described above. On days 7, 10 and 14 of culture, CAR$^+$ CD4$^+$ and CD8$^+$ cells were sorted, and RNA was isolated using Qiagen mRNEasy kit. Samples were library prepped and sequenced via Illumina NextSeq paired end platform by the Stanford Functional Genomics Core.

Bulk RNA-seq

For bulk RNA isolation, healthy donor T cells were prepared as described. On day 10 or 11 of culture, total mRNA was isolated from 2×10^6 bulk CAR T cells using Qiagen RNEasy Plus mini isolation kit. Bulk RNA-seq was performed by BGI America (Cambridge, MA) using the BGISEQ-500 platform, single-end 50-bp read length, at 30×10^6 reads per sample. Principal component analysis was performed using stats package and plots with ggplot2 package in R (version 3.5)[52]. GSEA was performed using the GSEA software (Broad Institute) as described[53,54]. DAVID analysis was performed for transcription factor enrichment as described[55,56].

Single-cell RNA-seq

To compare gene expression in single CD19-28z and GD2-28z CAR cells, we sorted naive T-cell subset on day 0 for subsequent single-cell analysis on day 10 using the Chromium platform (10X Genomics) and the Chromium Single Cell 3′ v2 Reagent Kit according to the manufacturer's instructions. cDNA libraries were prepared separately for CD19-CAR and GD2-CAR cells, and the CD4$^+$ cells and CD8$^+$ cells were combined in each run to be separated bioinformatically downstream. Sequencing was performed on the Illumina NextSeq system (paired-end, 26 bp into read 1 and 98 bp into read 2) to a depth of more than 100,000 reads per cell. Single-cell RNA-seq reads were aligned to the Genome Reference Consortium Human Build 38 (GRCh38), normalized for batch effects, and filtered for cell events using the Cell Ranger software (10X Genomics). A total of 804 CD19-CAR and 726 GD2-CAR T cells were sequenced to an average of 350,587 post-normalization reads per cell. The cell–gene matrix was further processed using the Cell Ranger R Kit software (10X Genomics) as previously described[57]. In brief, we first selected genes with at least one unique molecular identifier (UMI) counts in any given cell. UMI counts were then normalized to UMI sums for each cell and multiplied by a median UMI count across cells. Next, the data were transformed by taking a natural logarithm of the resulting data matrix. For correlation network of exhaustion-related transcription factors, transcription factor genes identified as differentially expressed ($P < 0.05$) by DESeq2 form the nodes of the network. Colours represent $\log_2$-transformed fold change (GD2 vs CD19 CAR). Edge thickness represents the magnitude of correlation in

expression between the relevant pair of genes across cells. Correlation score greater than 0.1 was used to construct networks.

To compare gene expression in single JUN-overexpressing and control Her2-BBz CAR T cells in vivo, live human CD45$^+$ tumour-infiltrating cells were sorted and pooled from six NSG mice bearing 143B osteosarcoma tumours 14 days after CAR T cell infusion. Sorted cells were analysed using the 10X Genomics platform as described above and sequenced on the Illumina HighSeq 4000 system to a depth of more than 50,000 reads per cell. A total of 6,946 Her2-BBz and 10,985 JUN-Her2-BBz cells were sequenced to an average of 49,542 post-normalization reads per cell. The cell–gene matrix was further processed using the Seurat v.3.0 software[58,59]. In brief, we selected genes expressed in ≥50 cells. Single live cells were selected as droplets expressing ≥500 genes with ≤20,000 UMI counts and ≤10% mitochondrial reads. UMI count data matrix was transformed and scaled, including variable feature selection, with SCTransform pipeline. T cells were selected as CD3$^+$ events (99.3% cells expressing *CD3G*, *CD3D*, *CD3E*, and/or *CD247* gene). Where indicated, CD4$^+$ and CD8$^+$ T cell subsets were selected (8.3% *CD4*$^+$ *CD8*$^-$, 70.3% *CD4*$^-$ *CD8*$^+$). The resulting data matrix was then examined using differential expression analysis, cell cycle analysis, clustering, and UMAP embedding.

Statistical analysis

Unless otherwise noted, statistical analyses for significant differences between groups were conducted using unpaired two-tailed *t*-tests without correction for multiple comparisons and without assuming consistent s.d. using GraphPad Prism 7. Survival curves were compared using the log-rank Mantel–Cox test. See Supplementary Table 2 for full statistical analyses, including exact *P* values, t-ratio, and degrees of freedom.

Reporting summary

Further information on research design is available in the Nature Research Reporting Summary linked to this paper.

Data availability

The sequencing datasets generated in this publication have been deposited in NCBI Gene Expression Omnibus (GEO)[60,61] and are accessible through GEO series accession numbers: bulk RNA-seq: GSE136891, scRNA-seq CD19/GD2-28z: GSE136874, scRNA-seq control/JUN-Her2-BBz TILs: GSE136805, ATAC-seq: GSE136796, ChIP–seq: GSE136853.

47. Hudecek, M. et al. The nonsignaling extracellular spacer domain of chimeric antigen receptors is decisive for in vivo antitumor activity. *Cancer Immunol. Res.* **3**, 125–135 (2015).
48. Jena, B. et al. Chimeric antigen receptor (CAR)-specific monoclonal antibody to detect CD19-specific T cells in clinical trials. *PLoS ONE* **8**, e57838 (2013).
49. Sotillo, E. et al. Coordinated activation of the origin licensing factor CDC6 and CDK2 in resting human fibroblasts expressing SV40 small T antigen and cyclin E. *J. Biol. Chem.* **284**, 14126–14135 (2009).
50. Nagaraja, S. et al. Transcriptional dependencies in diffuse intrinsic pontine glioma. *Cancer Cell* **31**, 635–652 (2017).
51. Corces, M. R. et al. An improved ATAC-seq protocol reduces background and enables interrogation of frozen tissues. *Nat. Methods* **14**, 959–962 (2017).
52. Wickham, H. *Ggplot2: Elegant Graphics for Data Analysis* (Springer, 2009).
53. Mootha, V. K. et al. PGC-1alpha-responsive genes involved in oxidative phosphorylation are coordinately downregulated in human diabetes. *Nat. Genet.* **34**, 267–273 (2003).
54. Subramanian, A. et al. Gene set enrichment analysis: a knowledge-based approach for interpreting genome-wide expression profiles. *Proc. Natl Acad. Sci. USA* **102**, 15545–15550 (2005).
55. Huang, W., Sherman, B. T. & Lempicki, R. A. Systematic and integrative analysis of large gene lists using DAVID bioinformatics resources. *Nat. Protoc.* **4**, 44–57 (2009).
56. Huang, W., Sherman, B. T. & Lempicki, R. A. Bioinformatics enrichment tools: paths toward the comprehensive functional analysis of large gene lists. *Nucleic Acids Res.* **37**, 1–13 (2009).
57. Zheng, G. X. et al. Massively parallel digital transcriptional profiling of single cells. *Nat. Commun.* **8**, 14049 (2017).
58. Butler, A., Hoffman, P., Smibert, P., Papalexi, E. & Satija, R. Integrating single-cell transcriptomic data across different conditions, technologies, and species. *Nat. Biotechnol.* **36**, 411–420 (2018).
59. Stuart, T. et al. Comprehensive integration of single-cell data. *Cell* **177**, 1888–1902 (2019).
60. Edgar, R., Domrachev, M. & Lash, A. E. Gene Expression Omnibus: NCBI gene expression and hybridization array data repository. *Nucleic Acids Res.* **30**, 207–210 (2002).
61. Barrett, T. et al. NCBI GEO: archive for functional genomics data sets—update. *Nucleic Acids Res.* **41**, D991–D995 (2013).

Acknowledgements This work was supported by a Stand Up To Cancer–St Baldrick's–National Cancer Institute Pediatric Dream Team Translational Cancer Research Grant (C.L.M.), the Parker Institute for Cancer Immunotherapy (C.L.M., H.Y.C., Z.G.), the Virginia and D.K. Ludwig Fund for Cancer Research (C.L.M.), and NIH P50-HG007735 (H.Y.C.). H.Y.C. is an Investigator of the Howard Hughes Medical Institute. A.T.S. was supported by a Parker Bridge Scholar Award from the Parker Institute for Cancer Immunotherapy and a Career Award for Medical Scientists from the Burroughs Welcome Fund. R.C.L. was supported by the Emerson Collective Cancer Research Fund. The Illumina HiSeq 4000 used here was purchased with the NIH funds (award S10OD018220). Figure 4a was created by S. Knemeyer, SciStories LLC.

Author contributions R.C.L. cloned the constructs, designed and performed experiments, analysed data, and wrote the manuscript. E.W.W. and E.S. designed and performed experiments. E.S. performed all immunoblots, immunoprecipitations and GSEAs. D.G., J.G., A.T.S. and H.Y.C. performed and analysed ATAC-seq. Z.G., C.F.A.d.B. and S.R.Q. performed and analysed single-cell RNA-seq. H.A. and R.J. performed and analysed bulk RNA-seq. J.L. and V.T. cloned the JUN-mutant and JUN-DD constructs and performed experiments. R.M. cloned the HA-GD2 CAR and created the CD19^{low} Nalm6. P.X. performed mouse injections and imaging. S.N. and M.M. performed ChIP–seq experiments and analysis. C.L.M. designed experiments and wrote the manuscript.

Competing interests C.L.M., R.C.L., E.W.W. and E.S. are inventors on a Stanford University Provisional patent pending on modulating AP-1 to enhance function of T cells; 62/599,299; C.L.M. is a founder of, holds equity in and receives consulting fees from Lyell Immunopharma, which has licensed the technology. R.C.L. is employed by and E.W.W. and E.S. are consultants for Lyell Immunopharma.

Additional information

Supplementary information is available for this paper at https://doi.org/10.1038/s41586-019-1805-z.

Correspondence and requests for materials should be addressed to C.L.M.

Peer review information *Nature* thanks Steven Albelda, Takeshi Egawa and the other, anonymous, reviewer(s) for their contribution to the peer review of this work.

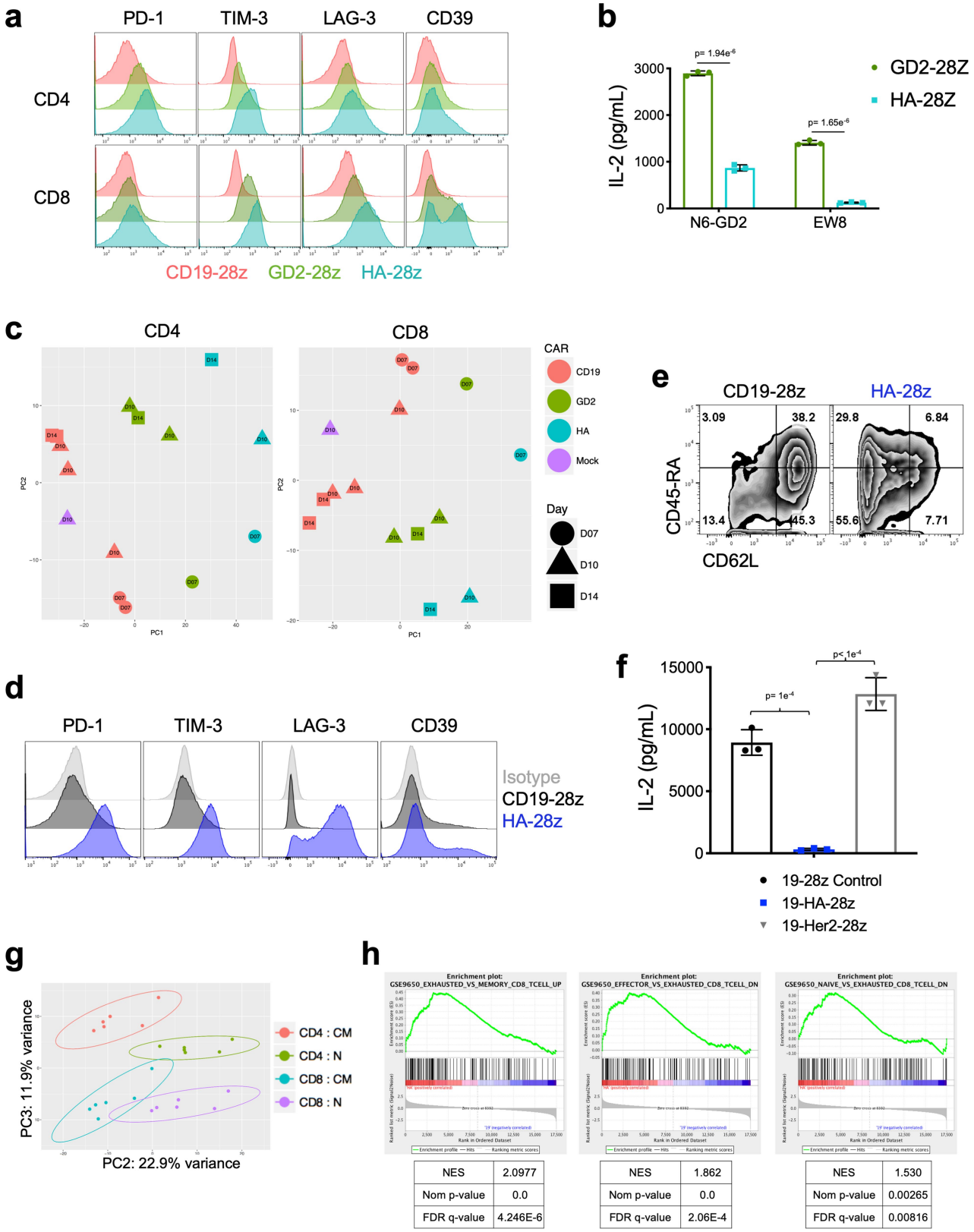

NES	2.0977
Nom p-value	0.0
FDR q-value	4.246E-6

NES	1.862
Nom p-value	0.0
FDR q-value	2.06E-4

NES	1.530
Nom p-value	0.00265
FDR q-value	0.00816

Extended Data Fig. 1 | See next page for caption.

Extended Data Fig. 1 | High-affinity 14g2a-GD2(E101K) CAR T cells manifest an exaggerated exhaustion signature compared with the original 14g2a-GD2 CAR T cells. a, Surface inhibitory receptor expression in CD19, GD2 and HA-GD2(E101K) CAR T cells at day 10 of culture. High-affinity E101K mutation results in increased inhibitory receptor expression in $CD4^+$ and $CD8^+$ CAR T cells, compared with parental GD2 CAR T cells. **b**, IL-2 secretion after 24h co-culture of HA-GD2(E101K) or original GD2-28z CAR T cells with $GD2^+$ target cells. The increased exhaustion profile of HA-GD2(E101K) CAR T cells corresponds to decreased functional activity, as measured by the ability to produce IL-2 after stimulation. Data are mean ± s.d. of triplicate wells; representative of four independent experiments. **c**, PCA of bulk RNA-seq demonstrates larger variance between HA-GD2(E101K) and CD19 CAR T cells, whereas GD2-28z (short hinge) CAR T cells are intermediary. Left, $CD4^+$ T cells. Right, $CD8^+$ CAR T cells, naive-derived. Number of replicates is indicated. **d**, **e**, HA-GD2(E101K) CAR expression causes enhanced inhibitory receptor expression (**d**) and decreased memory formation (**e**) in $CD4^+$ CAR T cells. (See Fig. 1 for $CD8^+$ data). **f**, IL-2 secretion from control CD19-28z CAR T cells or CD19 CAR T cells with bi-cistronic expression of tonically signalling HA-GD2(E101K) (19-HA-28z, blue) or bi-cistronic expression of Her2-28z (19-Her2-28z, grey) after 24-h stimulation with Nalm6 ($CD19^+GD2^-Her2^-$) target cells to demonstrate that co-expression of HA-GD2-28z CAR induces T cell dysfunction in CD19-28z CAR T cells. Data are mean ± s.d. of triplicate wells; representative of three independent experiments. **g**, RNA-seq PCA from Fig. 1 showing PC2 separation is driven by central memory versus naive starting subset and PC3 separation driven by CD4 versus CD8. **h**, Gene set enrichment analysis (GSEA): gene sets upregulated in day-10 HA-28z CAR T cells versus CD19-28z CAR T cells showed significant overlap with genes upregulated in exhausted versus memory $CD8^+$ cells (left), exhausted versus effector $CD8^+$ cells (middle), and exhausted versus naive $CD8^+$ cells (right) in a mouse model of chronic viral infection[4]. NES, normalized enrichment score. In **b** and **f**, *P* values determined by unpaired two-tailed *t*-tests.

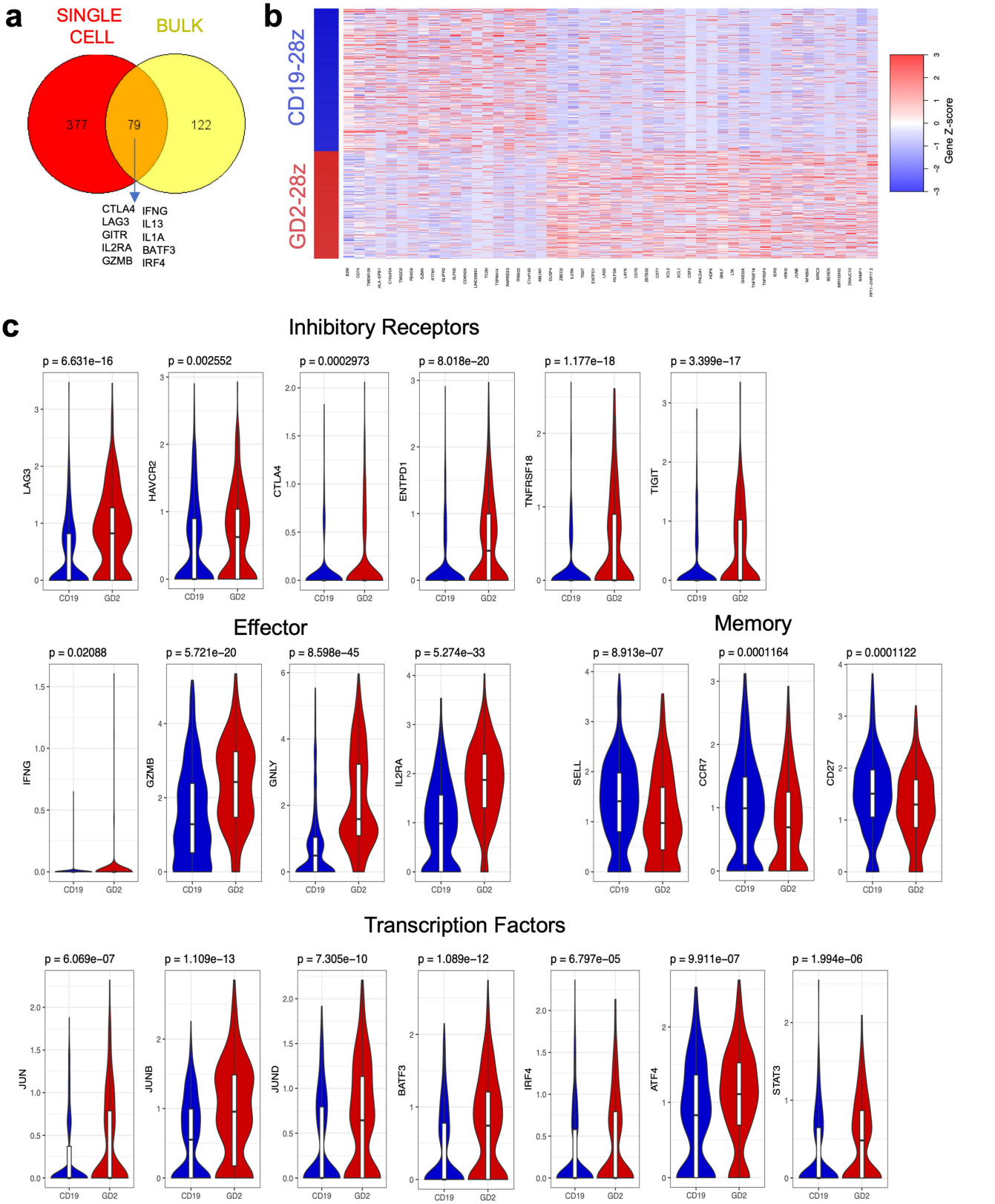

Extended Data Fig. 2 | GD2-28z CAR T cells display an exhaustion signature at the single cell-level. a, Venn diagram showing overlapping genes in differential expression analysis of single cell data (red) and the top 200 genes driving the separation of CD19 and HA-28z CAR T cells in bulk RNA-seq (yellow, Fig. 1f). In total, 79 out of the top 200 genes from bulk RNA-seq are differentially expressed by DESeq2 analysis in GD2-28z versus CD19-28z single cells. Highlighted genes from the intersection include inhibitory receptors (*CTLA4*, *LAG3*, *GITR*), effector molecules (*CD25*, *IFNG*, *GZMB*), cytokines (*IL13* and *IL1A*) and bZIP/IRF family transcription factors (*BATF3* and *IRF4*). **b**, Heat map clustering the top 50 differentially expressed genes in GD2-28z versus CD19-28z single-cell transcriptome analysis. Each row represents one cell. **c**, Violin plots depicting individual gene expression in $CD8^+$ GD2-28z and CD19-28z single CAR T cells. Genes upregulated in GD2 CAR T cells include inhibitory receptors, effector molecules and AP-1 family transcription factors, whereas CD19 CAR T cells have increased expression of memory-associated genes. *P* values determined by unpaired two-tailed Wilcoxon–Mann–Whitney *U* test.

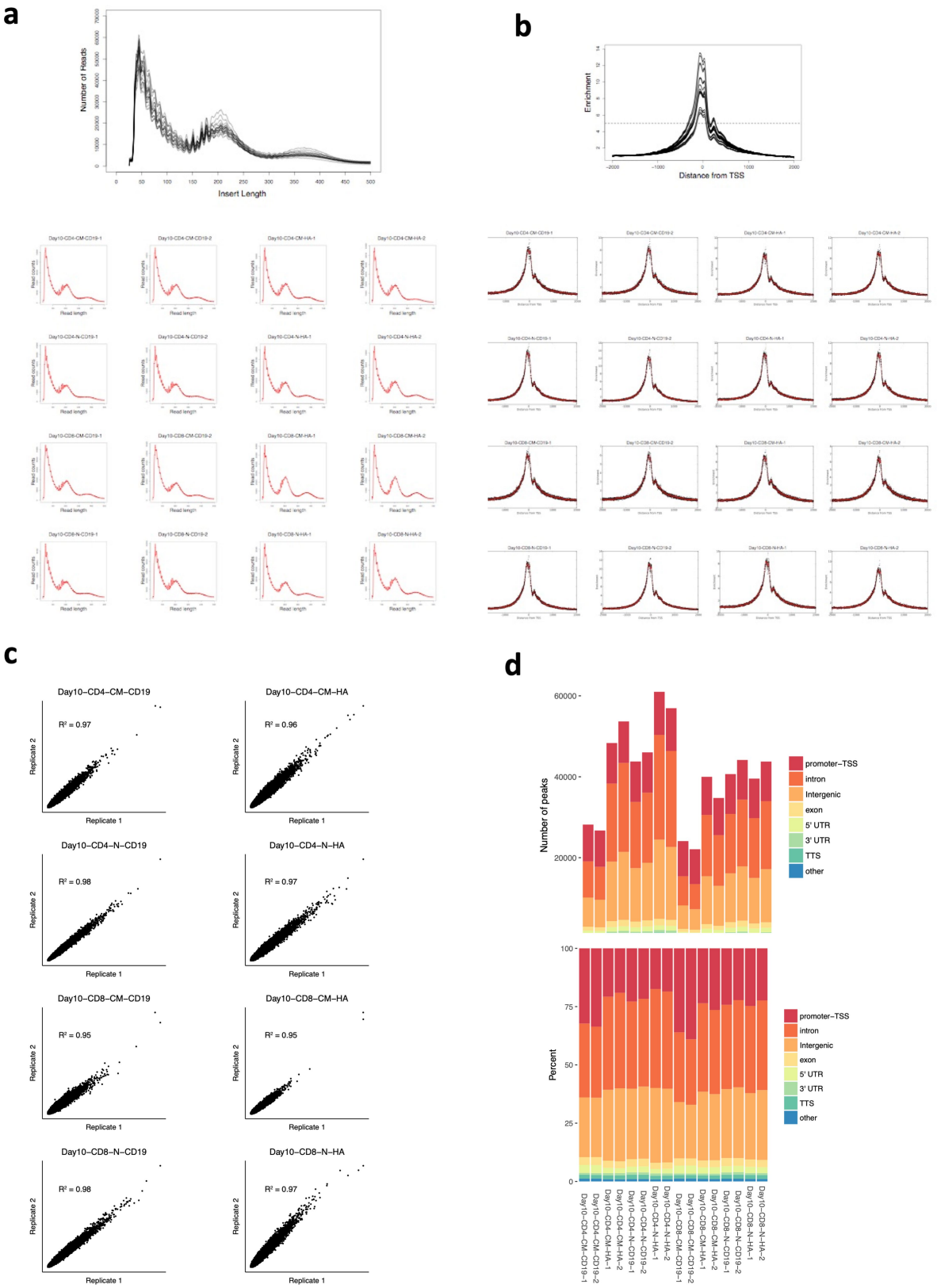

Extended Data Fig. 3 | ATAC-seq data quality control. a, **b**, Insert length (**a**) and insert distance (**b**) from transcriptional start site (TSS) for combined (top) and individual (bottom) samples. **c**, Correlation between replicate samples. **d**, Location of mapped peaks in each sample by total number of peaks (top) and frequency of total (bottom).

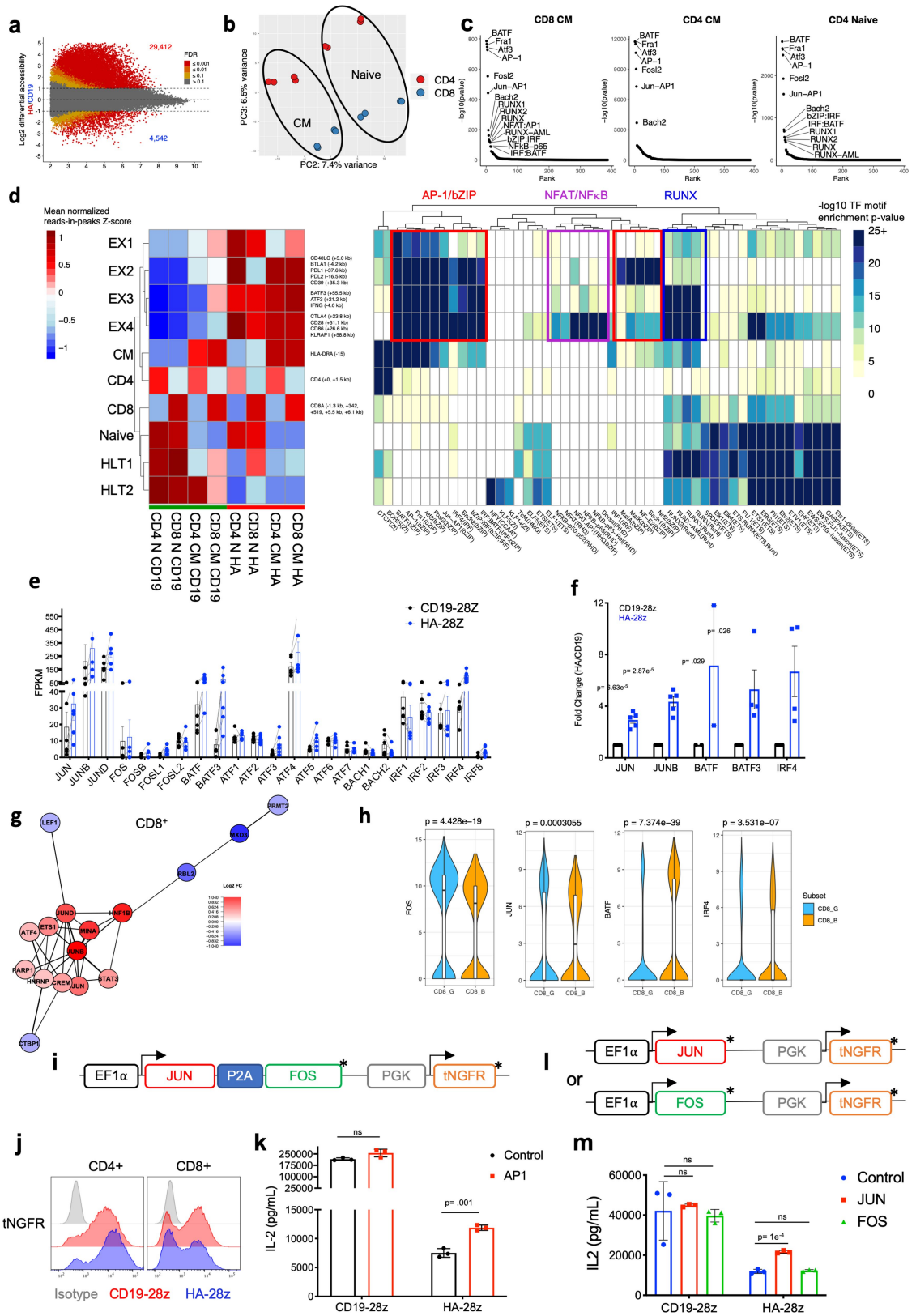

Extended Data Fig. 4 | See next page for caption.

Extended Data Fig. 4 | AP-1 family transcription factors in HA-28z exhausted CAR T cells. a, Differentially accessible chromatin regions in $CD4^+$ CD19-28z and HA-28z CAR T cells. Both the naive- and central-memory-derived subsets are incorporated for each CAR. **b**, PCA from Fig. 1h showing PC2 separation is driven by central memory versus naive, and PC3 separation driven by CD4 versus CD8. **c**, Top transcription factor motifs enriched in chromatin regions differentially accessible in HA-28z CAR T cells comprise AP-1–bZIP family factors in all starting T cell subsets. $CD8^+$ naive subset is shown in Fig. 2. **d**, Peak clustering by shared regulatory motif (left) and enrichment heat map of transcription factor motifs (right) in each cluster. Ten different clusters including clusters associated with exhausted (EX1–EX4) or healthy (HLT1–HLT2) CAR T cells, central memory or naive starting subset, and CD4 or CD8 T cell subset. Genes of interest in each cluster are highlighted to the right. **e**, Bulk RNA-seq expression (fragments per kilobase of exon model per million reads mapped, FPKM) of indicated AP-1–bZIP and IRF family members in CD19-28z (black) and HA-28z (blue) CAR T cells. Data are mean ± s.e.m. from $n = 6$ samples across three donors showing paired CD19 versus HA expression for each gene. $^*P < 0.05$, $^{**}P < 0.01$, $^{***}P < 0.001$, Wilcoxon matched-pairs signed rank test (see Supplementary Information for exact P values). **f**, Increased protein expression of c-Jun, JunB, BATF3 and IRF4 in HA-28z versus CD19-28z CAR T cells at day 10 of culture by immunoblotting. Densitometry measurements of the fold change in HA compared with CD19 ($n = 2$–5 experiments). P values determined by unpaired two-tailed t-tests. **g**, Correlation network of exhaustion-related transcription factor in naive-derived $CD8^+$ GD2-28z CAR T cells using single-cell RNA-seq analysis. **h**, Violin plots depicting single-cell gene expression of *FOS*, *JUN*, *BATF* and *IRF4* in $CD8^+$ clusters associated with response (CD8.G) and non-response (CD8.B) in patients with metastatic melanoma after checkpoint therapy (CD8T-post-CD8G.B)[29]. P values determined by unpaired two-tailed Wilcoxon–Mann–Whitney U test. In **i**–**m**, AP-1-modified HA-28z CAR T cells exhibit enhanced functional activity. **i**–**k**, CAR T cells were co-transduced with (AP-1) or without (control) a lentiviral vector encoding AP-1 transcription factors Fos and c-Jun and a truncated NGFR (tNGFR) surface selection marker. **i**, Schematic of the lentiviral construct. **j**, Representative transduction efficiency of AP-1-modified CAR T cells as measured by NGFR surface expression in indicated $CD4^+$ and $CD8^+$ CAR T cells. **k**, IL-2 production in control (black) or AP-1-modified (red) CAR T cells after 24-h stimulation with 143B-CD19 target cells. AP-1-modified HA-28z CAR T cells show increased IL-2 production compared with control CAR T cells. Data are mean ± s.d. of triplicate wells; representative of two independent experiments. **l**, **m**, CAR T cells were co-transduced with lentiviral vectors encoding either c-Fos or c-Jun and a tNGFR surface selection marker. **l**, Schematics of the c-Fos and c-Jun lentiviral constructs. **m**, IL-2 production in control (blue), Fos (green) or c-Jun (red) modified CAR T cells after 24-h stimulation with Nalm6-GD2 target cells. Data are mean ± s.d. of triplicate wells; representative of two independent experiments. Asterisk in **i** and **l** denotes a stop codon. P values determined by unpaired two-tailed t-tests. ns, not significant ($P > 0.05$).

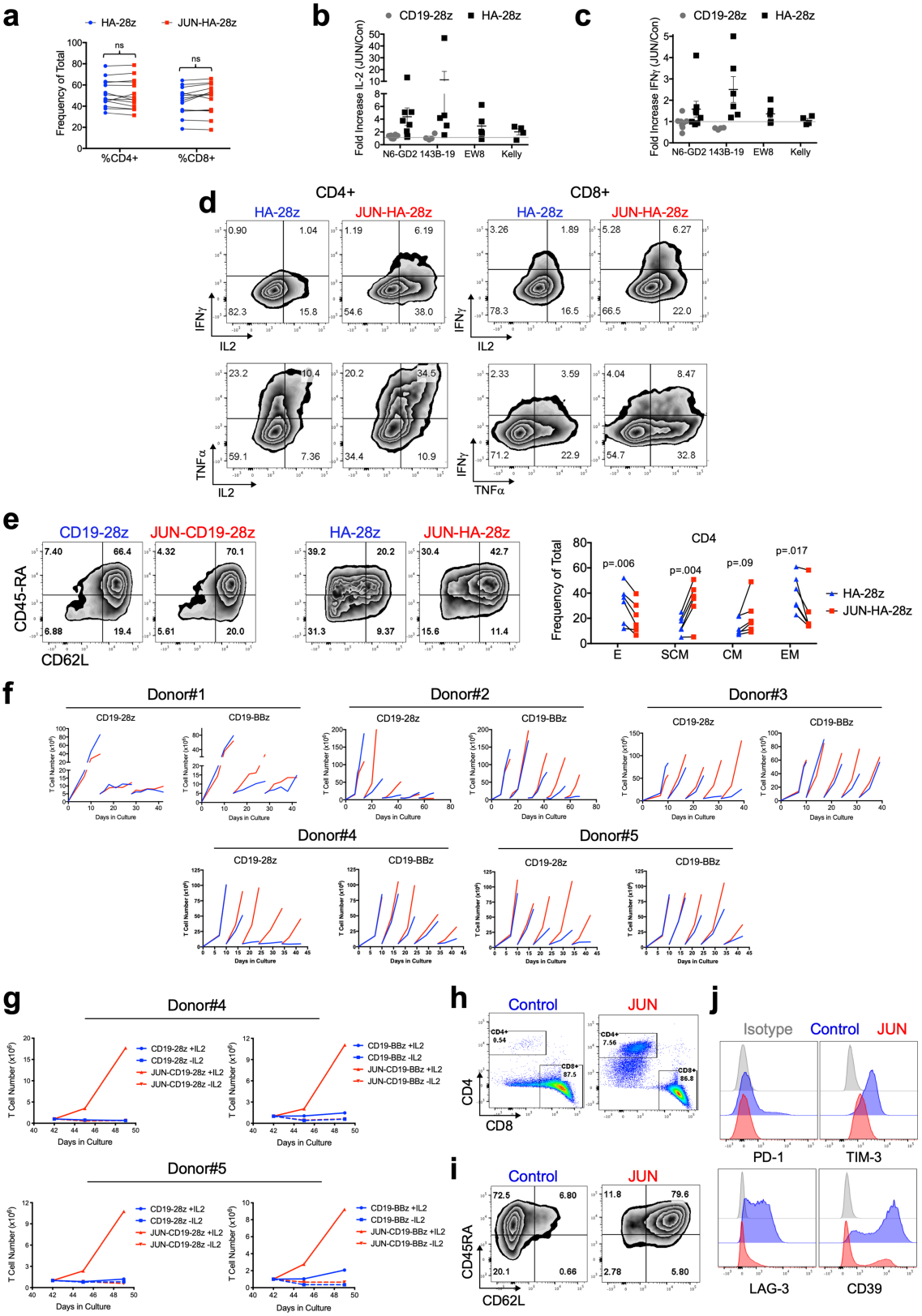

Extended Data Fig. 5 | See next page for caption.

Extended Data Fig. 5 | Enhanced activity of JUN-modified CAR T cells. JUN CAR T cells were produced as in Fig. 3. **a**, c-Jun overexpression does not affect the CD4:CD8 ratio in HA-28z CAR T cells at day 10 of culture ($n = 14$ independent experiments). Lines indicate paired samples from the same donor. *P* values determined by paired, two-tailed *t*-tests. **b**, **c**, Fold increase in IL-2 (**b**) and IFNγ (**c**) release after 24-h co-culture with the indicated target cells in JUN versus control CD19 and HA-28z CAR T cells. Each dot represents one independent experiment from different donors of $n = 8$ total experiments. **d**, Representative contour plots demonstrating increased intracellular cytokine production in both $CD4^+$ and $CD8^+$ JUN-HA-28z versus control HA-28z CAR T cells stimulated for 5 h with Nalm6-GD2 target cells. Representative of three independent experiments. **e**, Left, flow cytometry showing representative CD45RA and CD62L expression in control versus JUN CAR $CD4^+$ T cells at day 10. Right, relative frequency of effector ($CD45RA^+CD62L^-$), stem-cell memory ($CD45RA^+CD62L^+$), central memory ($CD45RA^-CD62L^+$), and effector memory ($CD45RA^-CD62L^-$) cells in $CD4^+$ control or JUN-HA-28z CAR T cells ($n = 6$ donors from independent experiments). Lines indicate paired samples from the same donor. *P* values determined by paired two-tailed *t*-tests. **f**, Extended in vitro expansion of control (blue) or JUN-modified (red) CD19 CAR T cells in five independent experiments with five different healthy donors. At the indicated time points, T cells were re-plated in fresh T cell media with 100 IU ml^{-1} IL-2. T cells were counted and fed to keep cells at 0.5×10^6 cells per ml every 2–3 days. For Donor-1, 5×10^6 viable T cells were re-plated on days 14 and 28. For Donor-2, 5×10^6 viable T cells were re-plated on days 14, 28, 42 and 56. For Donor-3, 5×10^6 viable T cells were re-plated on days 10, 17, 24 and 31. For Donor-4 and Donor-5, 5×10^6 viable T cells were re-plated on days 10, 17, 24 and 34. **g**, On day 42 of culture, 1×10^6 viable T cells from Donor-4 (top) and Donor-5 (bottom) were re-plated and cultured for 7 days with or without IL-2. **h**–**j**, Cell-surface phenotype of control or JUN-CD19-28z CAR T cells from Fig. 3g (Donor-3) on day 46 of culture. **h**, CD4 versus CD8 expression. **i**, Surface expression of CD45RA versus CD62L . **j**, Day 46 surface exhaustion marker expression in $CD8^+$ T cells.

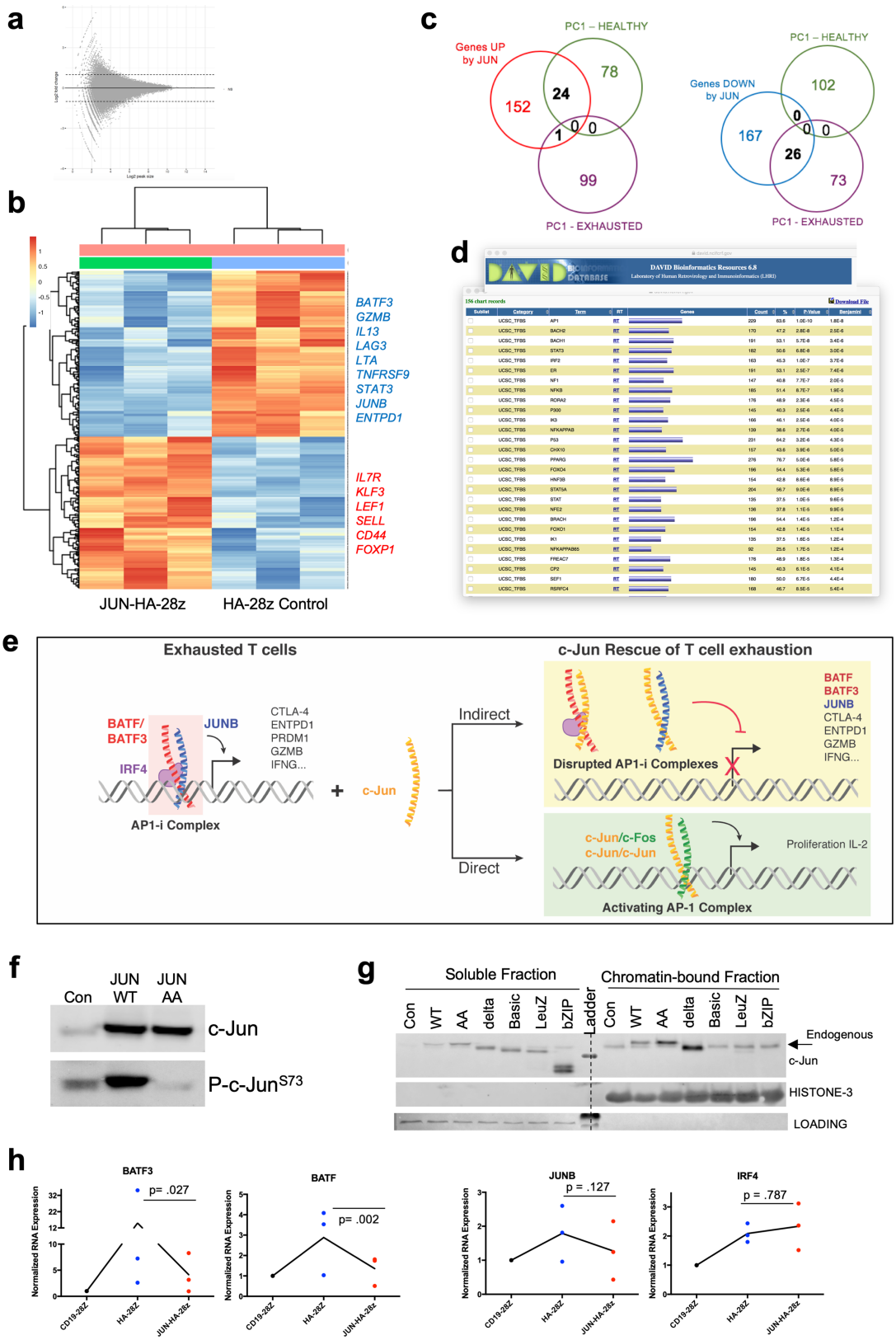

Extended Data Fig. 6 | See next page for caption.

Extended Data Fig. 6 | c-Jun overexpression mediates transcriptional but not epigenetic reprogramming of exhausted HA-28z CAR T cells. a, The log_2-transformed fold change in HA versus JUN-HA ATAC-seq demonstrating no significantly different peaks between conditions. **b**, Gene expression of 319 genes differentially expressed in JUN versus HA-28z CAR T cells (log_2-transformed fold change > 2, $P_{adj} < 0.05$). Genes downregulated in JUN CAR T cells (blue) include exhaustion-associated genes such as *BATF3*, *GZMB*, *LAG3*, *JUNB* and *ENTPD1* (encoding CD39). Genes upregulated in JUN CAR T cells (red) include genes associated with naive and memory differentiation such as *IL7R*, *LEF1*, *SELL* (CD62L), *CD44*, and *KLF3*. **c**, Venn diagrams showing overlap of the 319 genes differentially expressed in JUN versus HA-28z and the top 200 genes distinguishing exhausted (HA) and healthy (CD19) CAR T cells from PC1 in Fig. 1e, f. Genes downregulated in JUN CAR T cells overlap with exhaustion-associated (HA, PC1-exhausted) genes, and genes upregulated in JUN CAR T cells overlap with genes associated with healthy memory differentiation (CD19, PC1-healthy). **d**, DAVID bioinformatics analysis of transcription factor-binding sites within the 319 genes differentially expressed in JUN CAR T cells reveals that the top transcription factor binding motif belongs to the AP-1 family (269 out of 319 genes). **e**, Proposed mechanisms of c-Jun-mediated rescue of T cell exhaustion. AP-1i indicates an exhaustion-associated AP-1 complex. **f**, Immunoblot of total c-Jun and phosphorylated c-Jun (p-c-Jun^{S73}) in control, JUN-WT and JUN-AA HA-28z CAR T cells. **g**, Immunoblot analysis of c-Jun protein expression in control and indicated JUN-variant-expressing HA-28z CAR T cells in either soluble or chromatin-bound cellular lysate fractions. c-Jun variants with deletions in the C-terminal DNA binding and leucine zipper dimerization domains (basic, LeuZ and bZIP) cannot bind chromatin and do not rescue functional activity. **h**, Decrease in mRNA expression of *BATF*, *BATF3* and *JUNB* in JUN HA-28z CAR T cells compared with HA-28z cells ($n = 3$ donors, normalized to *CD19* mRNA). *P* values determined by ratio paired two-tailed *t*-test. See Supplementary Fig. 1 for gel source data.

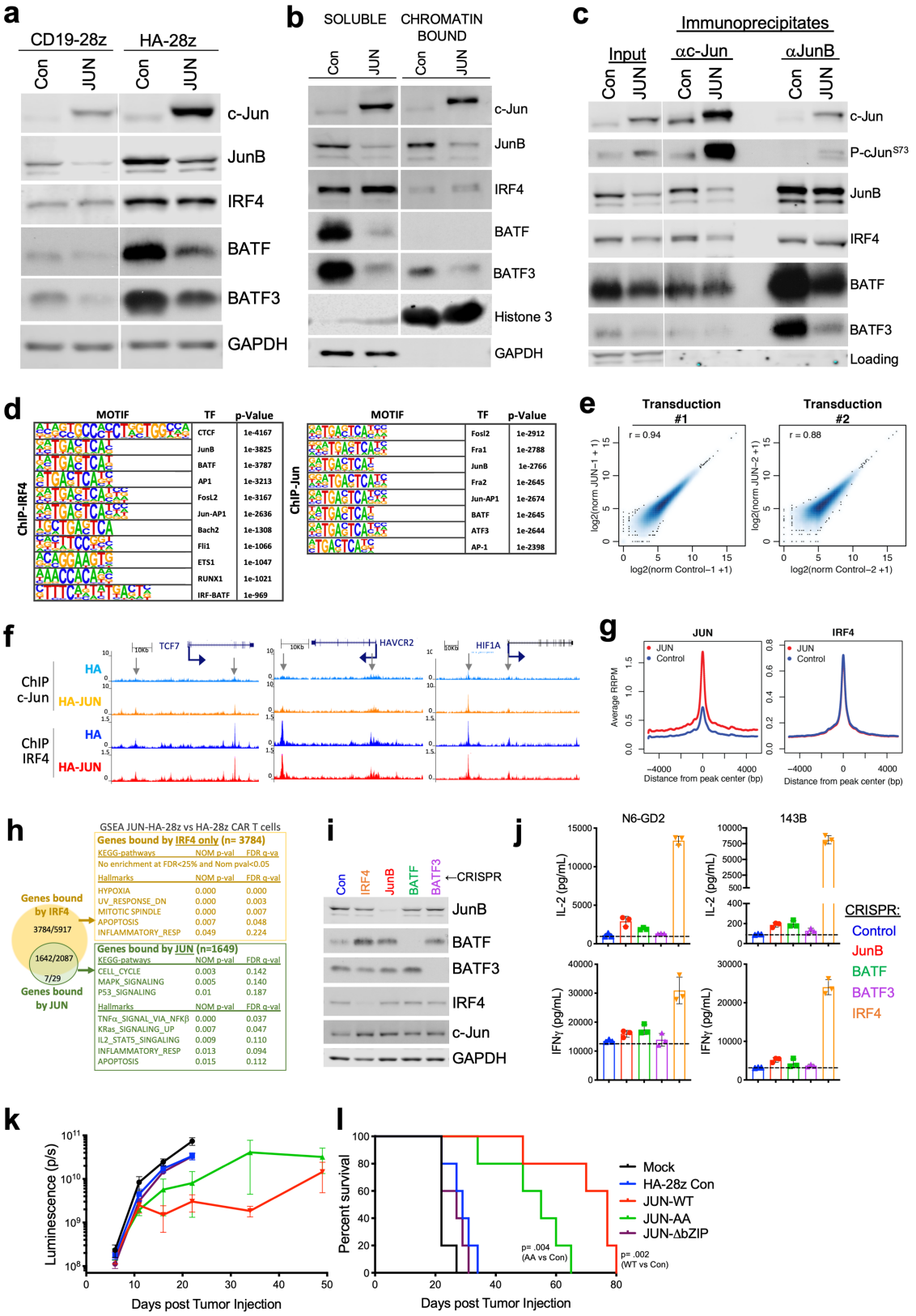

Extended Data Fig. 7 | See next page for caption.

Extended Data Fig. 7 | c-Jun overexpression decreases chromatin binding and complexing of JunB–BATF–BATF3–AP-1 complexes. a, Immunoblot analysis for the indicated AP-1–bZIP and IRF family member proteins in control and JUN CD19-28z and HA-28z CAR T cells (day 10). **b**, Immunoblot analysis for the indicated AP-1–bZIP and IRF family member proteins in control and JUN HA-28z CAR T cells (day 10) in either soluble or chromatin-bound cellular lysate fractions. **c**, c-Jun overexpression decreases JunB–BATF and JunB–BATF3 complexes by immunoprecipitation–immunoblot analysis. Input (left), immunoprecipitation for c-Jun (middle), or JunB (right) in control or JUN HA-28z CAR T cells. Levels of IRF4 protein and complexes with c-Jun are unchanged. **d**–**h**, ChIP–seq analysis for c-Jun and IRF4. **d**, Motif enrichment in IRF4-bound (left) or c-Jun-bound (right) loci. **e**, IRF4 signal genome-wide. Data shown for each transduction at all IRF4-bound sites. The *x* and *y* axes show log-transformed normalized count signal in control and JUN-overexpression cells, respectively. **f**, IRF4 and c-Jun ChIP–seq genome tracks in JUN or control HA-28z CAR T cells. c-Jun ChIP with reference exogenous genome (ChIP–Rx; top), with *x* axis representing genomic position and *y* axis representing reference-adjusted reads per million (RRPM). IRF4 ChIP (bottom), with *x* axis representing genomic position and *y*-axis representing reads per million (RPM). Arrows indicate peaks with increased c-Jun binding in HA-28z JUN cells at IRF4-bound sites within genes previously described to be regulated by IRF4 or BATF (*TCF7*, *HAVCR2* and *HIF1A*)[7]. **g**, Overexpressed c-Jun is bound to IRF4-occupied sites in the genome. Enrichment plot of c-Jun ChIP–Rx signal (left) or IRF4 ChIP–seq signal (right) in either JUN overexpression (red) or control (blue) HA-28z CAR T cells at all JUN-bound sites. The *x* axis shows distance from centre of JUN-bound site, and *y* axis shows average RRPM across replicates for c-Jun ChIP or average RPM across replicates for IRF4 ChIP. **h**, Venn diagram showing number of genes bound by IRF4 and/or c-Jun (*n* genes expressed/*n* genes bound). GSEA analysis with genes bound only by IRF4 (top) and genes bound by c-Jun and IRF4 (bottom), comparing levels of expression in JUN versus control HA-28z CAR T cells (normalized $P < 0.05$, FDR < 25%) **i**, Immunoblot of indicated AP-1 and IRF protein in control or CRISPR-knockout HA-28z CAR T cells demonstrating productive knockout of target protein. **j**, IL-2 (top) and IFNγ (bottom) release in HA-28z CAR T cells with control or CRISPR-knockout of the indicated AP-1 or IRF4 gene after 24 h stimulation with Nalm6-GD2 or 143B target cells. Data are mean ± s.d. of triplicate wells; representative of six independent experiments. Fold change across all experiments in Fig. 4e. In **k** and **l**, NSG mice were inoculated with 1×10^6 Nalm6-GD2 leukaemia cells via intravenous injection. A stress-test dose of 1×10^6 mock, HA-28z control, JUN-WT, JUN-AA or JUN-ΔbZIP HA-28z CAR^+ T cells was given intravenously on day 7. **k**, Tumour progression was monitored using bioluminescent imaging. **l**, JUN-WT and JUN-AA HA-28z CAR T cells enhanced long-term survival, and control and JUN-ΔbZIP HA-28z CAR T cells were almost non-functional compared with mock untransduced T cells at this dose. Data are mean ± s.e.m. of $n = 5$ mice per group. For gel source data see Supplementary Fig. 1.

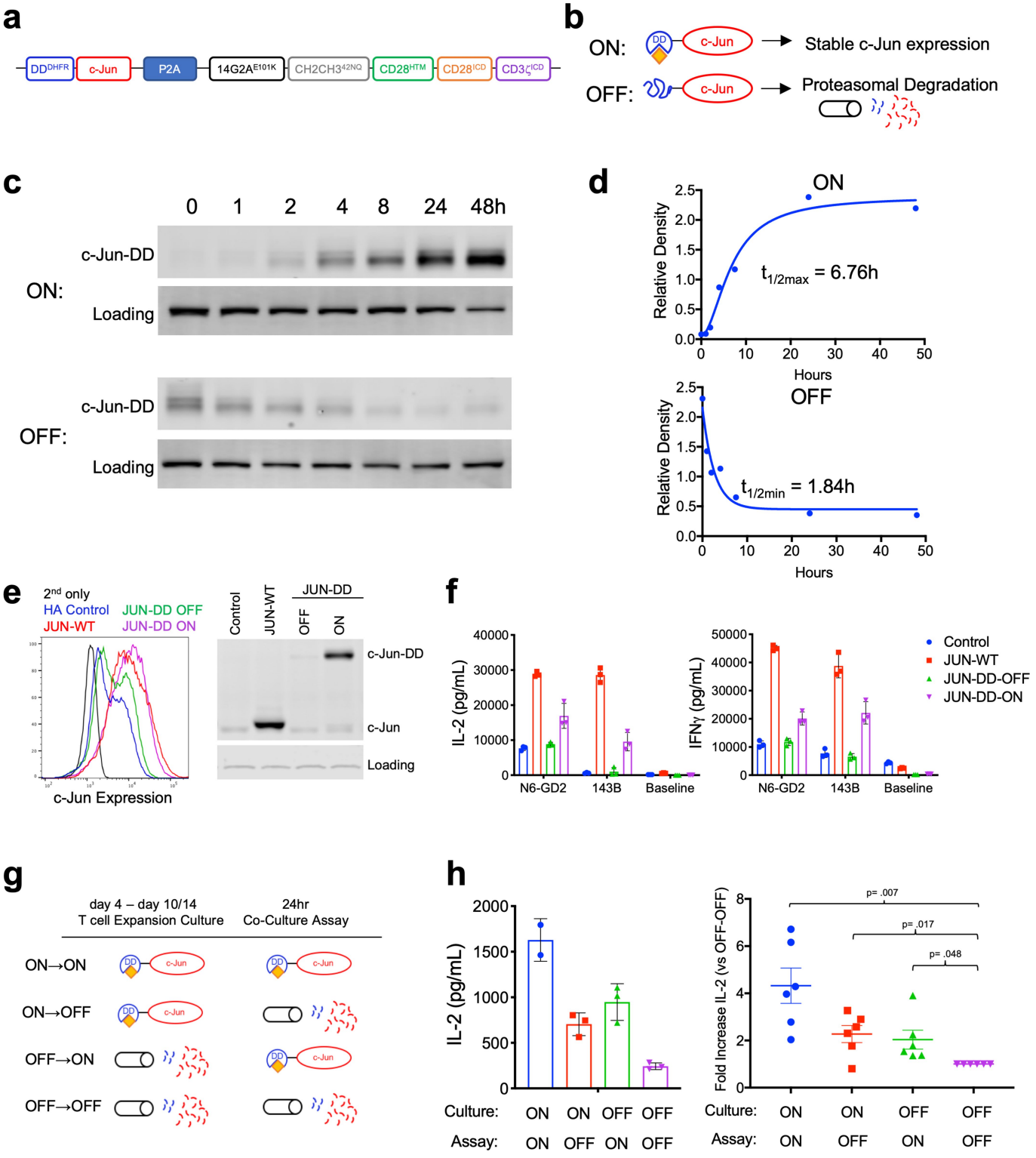

Extended Data Fig. 8 | See next page for caption.

Extended Data Fig. 8 | Functional rescue of exhausted HA-28z CAR T cells requires the presence of c-Jun during both chronic and acute T cell stimulation. a, Schematic of the destabilization domain (DD)-regulated JUN expression vector. **b**, Schematic of drug-induced stabilization of JUN-DD expression. Yellow diamond denotes trimethoprim (TMP)-stabilizing molecule. **c**, Kinetics of drug-induced c-Jun stability in JUN-DD CAR T cells as assessed by immunoblot. At time 0, 10 μM TMP was either added to untreated cells (ON) or washed out of previously treated cells (OFF). Cells were removed from each condition at 1, 2, 4, 8, 24 and 48 h and prepared for immunoblot analysis of c-Jun expression. The observed band corresponds to the size of JUN-DD. **d**, Densitometry analysis was performed on the blots from **c** and normalized to loading control. Expression was plotted against time and first-order kinetics curves were fit to the data to determine $t_{1/2}$ for OFF and ON kinetics. **e**, Total c-Jun expression in control, JUN-WT and JUN-DD HA-28z CAR T cells at day 10 by intracellular flow cytometry (left) and immunoblot (right). **f**, IL-2 (left) and IFNγ (right) production in control (blue), JUN-WT (red) or JUN-DD (OFF-green, ON-purple) modified HA-28z CAR T cells 24 h after stimulation with Nalm6-GD2 or 143B target cells, or media alone (baseline) at day 10. In **e** and **f**, OFF indicates without TMP, ON indicates T cells cultured in the presence of 10 μM TMP from day 4 and during co-culture. In **g** and **h**, TMP was added either during T cell expansion (starting at day 4) or only during co-culture with tumour cells as indicated in **g**. For ON-to-OFF and OFF-to-ON conditions, TMP was removed or added 18 h before co-culture to ensure complete c-Jun degradation or stabilization, respectively, before antigen exposure. **h**, IL-2 expression in one representative donor (left, s.d. across triplicate wells) and fold increase in IL-2 (s.e.m. of $n = 6$ independent experiments representing three different donors, relative to OFF–OFF condition). *P* values determined by unpaired two-tailed *t*-tests. For gel source data, see Supplementary Fig. 1.

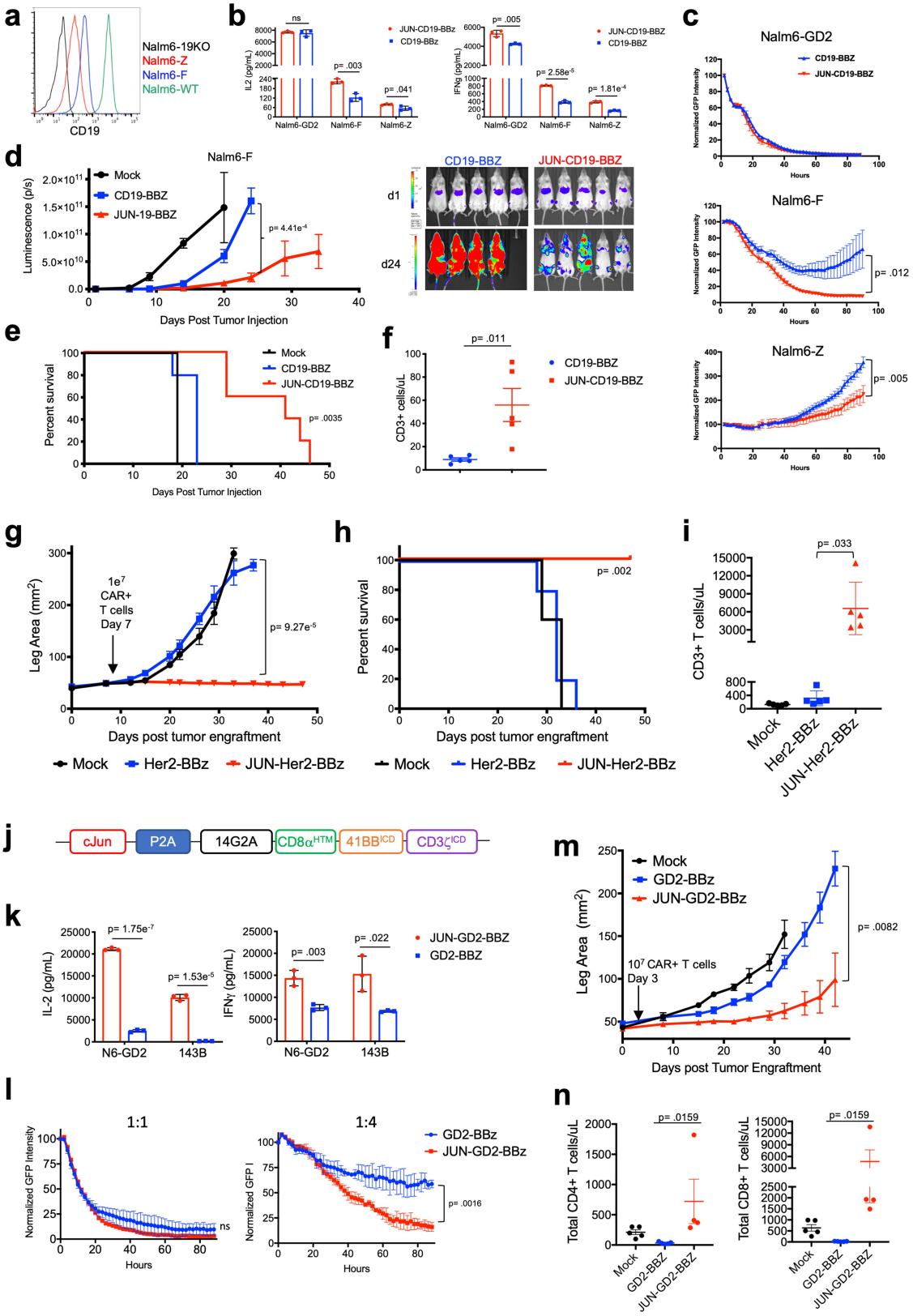

Extended Data Fig. 9 | See next page for caption.

Extended Data Fig. 9 | c-Jun overexpression enhances CD19-BBz CAR T cells activity under suboptimal antigen stimulation and Her2 or GD2-BBz CAR T cell function in solid tumours. a, CD19 surface expression on parental Nalm6-WT (green), CD19-knockout Nalm6 (19KO, black), and two different CD19-low Nalm6 clones (F and Z) Nalm6-19KO plus CD19^{low}-F (F; blue), and Nalm6-19KO plus CD19 ^{low}-Z (red). **b**, IL-2 (left) and IFNγ (right) release after co-culture of control (blue) or JUN (red) CD19-BBz CAR T cells exposed to Nalm6-WT and Nalm6-19^{low} clones F and Z. **c**, JUN versus control CD19-BBz CAR T cell lysis of GFP$^+$ Nalm6-WT (top), Nalm6-F (middle) or Nalm6-Z (bottom) target cells at a 1:2 effector:target cell ratio, demonstrating enhanced activity of JUN CAR T cells at low antigen density. Data in **b** and **c** denote mean ± s.d. of triplicate wells; representative of four independent experiments. In **d**–**f**, NSG mice were inoculated with 1×10^6 Nalm6-19^{low} clone F leukaemia cells. On day 1, 3×10^6 control or JUN CD19-BBz CAR$^+$ T cells or 3×10^6 mock0transduced T cells were transferred intravenously. **d**, Tumour growth was monitored by bioluminescent imaging. **e**, JUN expression significantly improved the long-term survival of CAR-treated mice. **f**, Mice receiving JUN-CD19-BBz CAR T cells display increased peripheral blood T cells on day 20. Data in **d**–**f** denote mean ± s.e.m. of $n = 5$ mice per group; representative of three independent experiments. Long-term tumour-free survival is impeded in this model owing to outgrowth of CD19-negative disease. In **g**–**i**, NSG mice were inoculated with 1×10^6 143B osteosarcoma cells via intramuscular injection; then, 1×10^7 mock, Her2-BBz or JUN-Her2-BBz CAR T cells were given intravenously on day 7. **g**, Tumour growth was monitored by caliper measurements. **h**, Long-term survival. **i**, On day 20 after tumour implantation, peripheral blood T cells were quantified in mice treated as in **g**. Data are mean ± s.e.m. of $n = 5$ mice per group; representative of two independent experiments. **j**, Vector schematic of JUN-GD2-BBz retroviral vector construct. **k**, IL-2 (left) and IFNγ (right) production in JUN-modified (red) or control (blue) GD2-BBz CAR T cells after 24 h stimulation with Nalm6-GD2 or 143B target cells. **l**, GD2-BBz CAR T cell lysis of GFP$^+$ Nalm6-GD2 target cells at 1:1 (left) or 1:4 (right) effector:target cell ratio. Data in **k** and **l** denote mean ± s.d. of triplicate wells; representative of four independent experiments. In **m** and **n**, NSG mice were inoculated with 0.5×10^6 143B-19 osteosarcoma cells via intramuscular injection; then, 1×10^7 mock, GD2-BBz or JUN-GD2-BBz CAR T cells were given intravenously on day 3. **m**, Tumour growth was monitored by caliper measurements. **n**, Peripheral blood CD4$^+$ (left) or CD8$^+$ (right) T cell counts at day 14 after tumour engraftment. Data are mean ± s.e.m. of $n = 5$ mice per group; representative of two independent experiments although early deaths (unrelated to tumour size) precluded survival curves in both models. *P* values in **n** were determined by a Mann–Whitney test. All other *P* values determined by unpaired two-tailed *t*-tests. Survival curves were compared using the log-rank Mantel–Cox test.

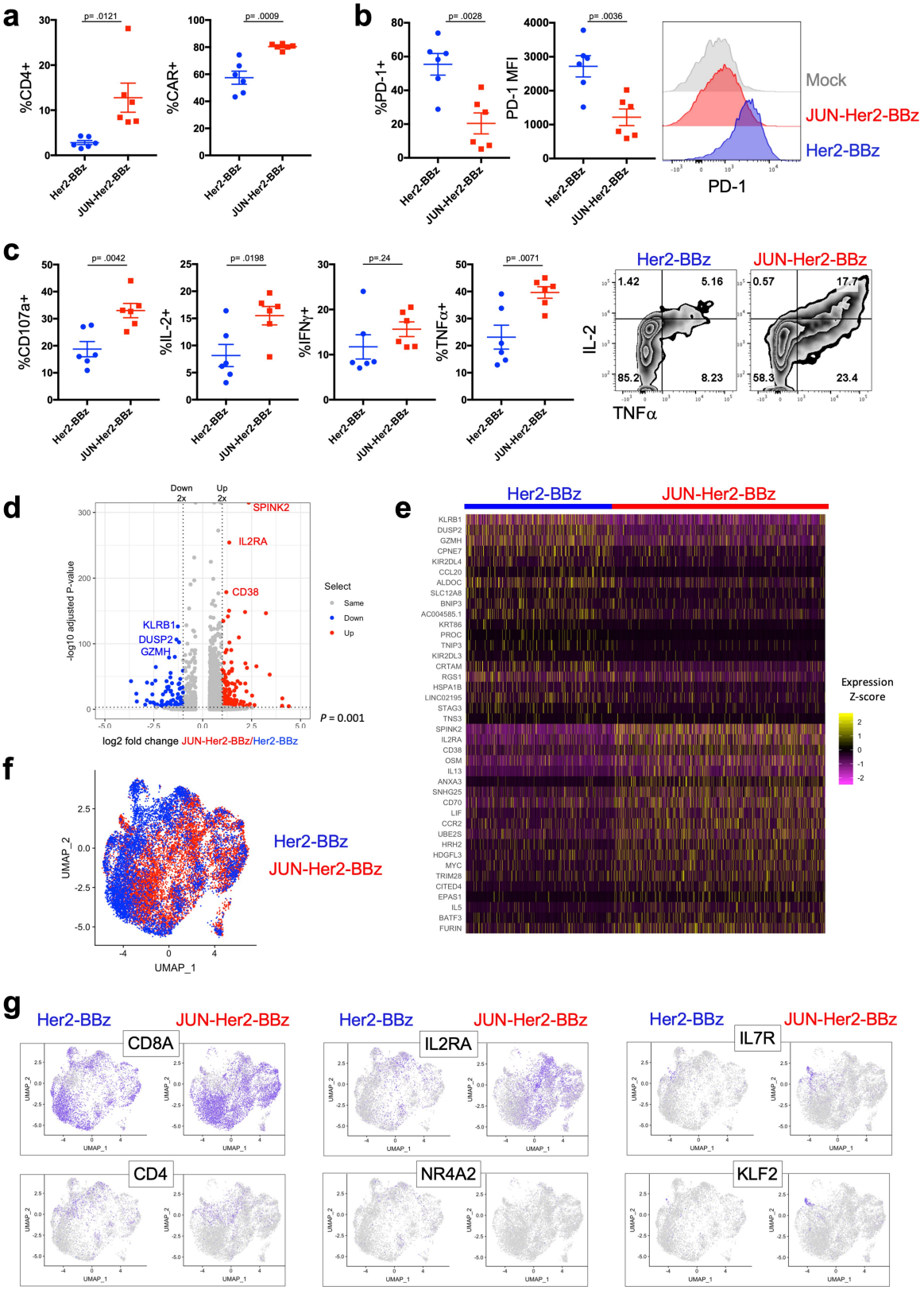

Extended Data Fig. 10 | See next page for caption.

Extended Data Fig. 10 | c-Jun overexpressing CAR TILs demonstrate increased activity in osteosarcoma xenograft tumours. Experimental design described in Fig. 6. **a**–**c**, Frequency (**a**), phenotype (**b**) and ex vivo functional activity (**c**) of $CD4^+$ TILs from mice treated with Her2-BBz or JUN-Her2-BBz CAR T cells. **a**, Left, $CD4^+$ levels as a proportion of total live tumour cells. Right, CAR^+ as a frequency of total live $CD4^+$. **b**, Percentage of $PD\text{-}1^+$ (left) and PD-1 mean fluorescence intensity (MFI; middle) of total live $CD4^+$ with representative flow histograms (right). Mock untransduced T cells were from spleens of tumour-bearing mice at the same time point. **c**, Frequency of indicated cytokine- or CD107a-producing cells after 5-h re-stimulation with Nalm6-$Her2^+$ target cells. Gated on total, live $CD4^+$ T cells (left) with representative contour plots (right). Data are mean ± s.e.m. of $n = 6$ mice per group. Each data point represents an individual mouse. *P* values determined by unpaired two-tailed *t*-tests. In **d**–**g**, dissociated tumour cell suspensions were labelled and sorted by FACS analysis to isolate live, human $CD45^+$ TILs. Sorted cells from six mice per group were pooled and approximately 10,000 cells were processed for 3′ single-cell RNA-seq on the 10X Genomics platform. **d**, Volcano plot showing results of differential expression analysis comparing JUN-Her2-BBz CAR T cells with control Her2-BBz CAR T cells. Top three upregulated and downregulated genes are highlighted. **e**, Heat map of the top 20 most significantly upregulated and downregulated genes. **f**, Uniform manifold approximation and projection (UMAP) embedding analysis showing JUN-Her2-BBz and control Her2-BBz CAR T cells overlaid. **g**, Expression of indicated transcripts in JUN-Her2-BBz or control Her2-BBz CAR T cells showing localization of $CD4^+$ and $CD8^+$ subsets, activation marker (*IL2RA*), exhaustion marker (*NR4A2*), and maintenance of a small memory-like population (*IL7RA*, *KLF2*) in JUN-overexpressing Her2-BBz CAR T cells within the solid osteosarcoma tumour microenvironment.

nature research

Corresponding author(s): Crystal L. Mackall

Reporting Summary

Nature Research wishes to improve the reproducibility of the work that we publish. This form provides structure for consistency and transparency in reporting. For further information on Nature Research policies, see Authors & Referees and the Editorial Policy Checklist.

Statistical parameters

When statistical analyses are reported, confirm that the following items are present in the relevant location (e.g. figure legend, table legend, main text, or Methods section).

n/a	Confirmed	
☐	☒	The exact sample size (*n*) for each experimental group/condition, given as a discrete number and unit of measurement
☐	☒	An indication of whether measurements were taken from distinct samples or whether the same sample was measured repeatedly
☐	☒	The statistical test(s) used AND whether they are one- or two-sided *Only common tests should be described solely by name; describe more complex techniques in the Methods section.*
☐	☐	A description of all covariates tested
☐	☒	A description of any assumptions or corrections, such as tests of normality and adjustment for multiple comparisons
☐	☒	A full description of the statistics including central tendency (e.g. means) or other basic estimates (e.g. regression coefficient) AND variation (e.g. standard deviation) or associated estimates of uncertainty (e.g. confidence intervals)
☐	☒	For null hypothesis testing, the test statistic (e.g. *F*, *t*, *r*) with confidence intervals, effect sizes, degrees of freedom and *P* value noted *Give P values as exact values whenever suitable.*
☒	☐	For Bayesian analysis, information on the choice of priors and Markov chain Monte Carlo settings
☒	☐	For hierarchical and complex designs, identification of the appropriate level for tests and full reporting of outcomes
☒	☐	Estimates of effect sizes (e.g. Cohen's *d*, Pearson's *r*), indicating how they were calculated
☐	☒	Clearly defined error bars *State explicitly what error bars represent (e.g. SD, SE, CI)*

Our web collection on statistics for biologists may be useful.

Software and code

Policy information about availability of computer code

Data collection	FACSDiva ver8.0.1 (BD Biosciences) for flow cytometry data acquisition. LivingImage ver4.5 (Perkin Elmer) for IVIS Spectrum bioluminescent imaging acquisition. Image Studio Software ver3.1 (LI-COR) for image acquisition of western blots. Incucyte ZOOM ver2016B (Essen BioScience) for incucyte image acquisition (killing assay).

Data analysis	FlowJo ver 10.4.2 for analysis of flow cytometry. GSEA ver 2.0 (Broad Institute, UCSD) for gene set enrichment analysis. GraphPad Prism ver 7.0 (GraphPad) for biostatistical analysis and scientific graphing. Excel ver 16.14.1 (Microsoft) for spreadsheet management. SnapGene ver 4.2.1 (GSL Biotech LLC) for vector visualization and cloning. ImageJ ver 1.51J (NIH) for densitometry image analysis. LivingImage ver4.5 (Perkin Elmer) for IVIS Spectrum bioluminescent imaging analysis. Incucyte ZOOM ver2016B (Essen BioScience) for incucyte image analysis and quantification. DESeq2 (version 2.1.24) and ggplot2 (Version 3.2.1)package in R (ver 3.5.0) for PCA and plots of bulk RNA-seq data. For single cell RNA-seq analysis: CD19-28z vs. GD2-28z: Cell Ranger (version 1.2.0), R Studio (version 1.1.453), R (version 3.5.0), and packages: cellrangerRkit (version 2.0.0) dplyr (version 0.7.6) DESeq2 (version 1.20.0) GO.db (version 3.6.0) org.Hs.eg.db (version 3.6.0) gplots (version 3.0.1) pheatmap (version 1.0.10) and igraph (version 1.2.1). ggplot2 (version 3.0.0); Her2-BBz vs. JUN-Her2-BBz: Cell Ranger (version 3.0.2), R Studio (version 1.1.456), R (version 3.5.2), future (version 1.14.0), sctransform (version 0.2.0), gplots (version 3.0.1.1), Seurat (version 3.0.3.9035), dplyr (version 0.8.3), reshape2 (version 1.4.3), ggplot2 (version 3.2.1). For ATAC-seq analysis: SeqPurge, Bowtie2 (Johns Hopkins, ver2.1.0), Picard tools (Broad Institute, ver 1.79), And the following packages in R: MACS2 (ver 2.1.0.20150731), Bedtools, Motifmatchr , rtracklayer, DESEq2 (ver 1.20.0), and ChromVAR. ENCODE hg19 blacklist (UCSC genome browser), HOMER Motif Analysis ver 4.9 (UCSD). chromVAR ver 1.60.

For manuscripts utilizing custom algorithms or software that are central to the research but not yet described in published literature, software must be made available to editors/reviewers upon request. We strongly encourage code deposition in a community repository (e.g. GitHub). See the Nature Research guidelines for submitting code & software for further information.

Data

Policy information about availability of data

All manuscripts must include a data availability statement. This statement should provide the following information, where applicable:

- Accession codes, unique identifiers, or web links for publicly available datasets
- A list of figures that have associated raw data
- A description of any restrictions on data availability

The sequencing datasets generated in this publication have been deposited in NCBI's Gene Expression Omnibus and are accessible through GEO Series accession numbers: bulk RNA-seq: GSE136891, scRNA-seq CD19/GD2-28z: GSE136874, scRNA-seq Control/JUN-Her2-BBz TILs: GSE136805, ATAC-seq: GSE136796, ChIP-seq: GSE136853. Data Figures associated with these datasets are Figures 1, 2, and 6 and Extended Data Figures 1,2,3,4,6,7, and 10.

Field-specific reporting

Please select the best fit for your research. If you are not sure, read the appropriate sections before making your selection.

☒ Life sciences ☐ Behavioural & social sciences ☐ Ecological, evolutionary & environmental sciences

For a reference copy of the document with all sections, see nature.com/authors/policies/ReportingSummary-flat.pdf

Life sciences study design

All studies must disclose on these points even when the disclosure is negative.

Sample size	Our established animal models consistently yield low variance, and difference in the means between groups greater than 50%. Power calculation estimates determined that 5 animals per group was sufficient to determine statistical significance.
Data exclusions	No data were excluded from analysis
Replication	In vivo experiments were replicated at least 2 times with independent experiments (as stated in the figure legends) with similar results. All replication results provided the same trends and conclusions. As noted, long-term tumor-free survival in the Nalm6-GD2 model (Figure 5) was impacted due to outgrowth of GD2(-) clones in some experiments. In vitro experiments were typically run with triplicate technical replicates and were reproduced at least 3 times in independent experiments (as stated in the figure legends) with similar results.
Randomization	For in vivo tumor models, mice were randomized to ensure equal mean tumor burden before T cell transfer.
Blinding	Investigators were blinded during in vivo tumor measurement. Otherwise, fully informed data analysis was performed. Fully blinded experiments were not possible due to personnel availability to accommodate such situations.

Reporting for specific materials, systems and methods

Materials & experimental systems

n/a	Involved in the study
[ ]	[x] Unique biological materials
[ ]	[x] Antibodies
[ ]	[x] Eukaryotic cell lines
[x]	[ ] Palaeontology
[ ]	[x] Animals and other organisms
[ ]	[x] Human research participants

Methods

n/a	Involved in the study
[ ]	[x] ChIP-seq
[ ]	[x] Flow cytometry
[x]	[ ] MRI-based neuroimaging

Unique biological materials

Policy information about availability of materials

Obtaining unique materials: Reagents (vector constructs) developed in house during this study are available upon request from the corresponding author.

Antibodies

Antibodies used: From BioLegend: CD4-APC-Cy7 (clone OKT4), CD8-PerCp-Cy5.5 (clone SK1), TIM3-BV510 (clone F38-2E2), CD39-FITC or APC-Cy7 (clone A1), CD95-PE (clone DX2), CD3-PacBlue (clone HIT3a), CD107a-BV607 (Clone H4A3), IL2-PECy7 Clone MQ1-17H12, IFNg-APC/Cy7 Clone 4S.B3, and TNFa-BV711 Clone Mab11.
From eBioscience: PD1-PE-Cy7 (clone eBio J105), LAG3-PE (clone 3DS223H), CD45RO-PE-Cy7 (clone UCHL1), CD45-PerCp-Cy5.5 (clone HI30),
From BD: CD45RA-FITC or BV711 (clone HI100), CCR7-BV421 (clone 150503), CD122-BV510 (clone Mik-ß3), CD62L-BV605 (clone DREG-56), CD4-BUV395 (clone SK3), CD8-BUV805 (clone SK1).
1A7 obtained from NCI-Frederick, CD19-Idiotype provided by Laurence Cooper.
For western blot: Cell Signaling: GAPDH (D46CR), Histone-3 (1B1B2), c-Jun (60A8), P-c-JunSer73 (D47G9), JunB(C37F9), BATF(D7C5) and IRF4(4964). The BATF3 (AF7437) antibody was from R&D. The b-Actin (Clone AC-15)-HRP conjugated was from Sigma-Aldrich.

Validation: All antibodies used for flow cytometry were validated by the manufacturer directly in human peripheral blood mononuclear cells. In our laboratory, antibody-specific staining was compared to isotype and no staining control samples.
CD4-APC-Cy7 (clone OKT4) was validated here https://www.biolegend.com/en-us/products/apc-cyanine7-anti-human-cd4-antibody-3658
CD8-PerCp-Cy5.5 (clone SK1) was validated here https://www.biolegend.com/en-us/products/percp-cyanine5-5-anti-human-cd8-antibody-6389
TIM3-BV510 (clone F38-2E2) was validated here https://www.biolegend.com/en-us/search-results/brilliant-violet-510-anti-human-cd366-tim-3-antibody-12009
CD39-FITC or APC-Cy7 (clone A1) was validated here https://www.biolegend.com/en-us/products/fitc-anti-human-cd39-antibody-4363
CD95-PE (clone DX2) was validated here https://www.biolegend.com/en-us/products/pe-anti-human-cd95-fas-antibody-643
CD3-PacBlue (clone HIT3a) was validated here https://www.biolegend.com/ja-jp/search-results/pacific-blue-anti-human-cd3-antibody-6505
CD107a-BV607 (Clone H4A3) was validated here https://www.biolegend.com/en-us/products/pe-anti-human-cd107a-lamp-1-antibody-4967
IL2-PECy7 Clone MQ1-17H12 was validated here https://www.biolegend.com/en-gb/products/pe-cy7-anti-human-il-2-antibody-6513
IFNg-APC/Cy7 Clone 4S.B3 was validated here https://www.biolegend.com/en-us/products/apc-anti-human-ifn-gamma-antibody-1012
TNFa-BV711 Clone Mab11 was validated here https://www.biolegend.com/en-us/products/brilliant-violet-711-anti-human-tnf-alpha-antibody-9034
PD1-PE-Cy7 (clone eBio J105) was validated here https://www.thermofisher.com/antibody/product/CD279-PD-1-Antibody-clone-eBioJ105-J105-Monoclonal/25-2799-42
LAG3-PE (clone 3DS223H) was validated here https://www.thermofisher.com/antibody/product/CD223-LAG-3-Antibody-clone-3DS223H-Monoclonal/12-2239-42
CD45RO-PE-Cy7 (clone UCHL1)was validated here https://www.thermofisher.com/antibody/product/CD45RO-Antibody-clone-UCHL1-Monoclonal/25-0457-42
CD45-PerCp-Cy5.5 (clone HI30)was validated here http://www.bdbiosciences.com/us/applications/research/stem-cell-research/cancer-research/human/percp-cy55-mouse-anti-human-cd45-hi30/p/564105
CD45RA-FITC or BV711 (clone HI100) was validated here http://www.bdbiosciences.com/eu/applications/research/t-cell-immunology/regulatory-t-cells/surface-markers/human/bv711-mouse-anti-human-cd45ra-hi100/p/563733
CCR7-BV421 (clone 150503)was validated here https://www.bdbiosciences.com/us/applications/research/t-cell-immunology/th-2-cells/surface-markers/human/bv421-mouse-anti-human-cd197-ccr7-150503/p/562555
CD122-BV510 (clone Mik-b3)was validated here http://www.bdbiosciences.com/us/applications/research/t-cell-immunology/regulatory-t-cells/surface-markers/human/bv510-mouse-anti-human-cd122-mik-3/p/563093
CD62L-BV605 (clone DREG-56)was validated here http://www.bdbiosciences.com/us/applications/research/t-cell-immunology/regulatory-t-cells/surface-markers/human/bv605-mouse-anti-human-cd62l-dreg-56/p/562720
CD4-BUV395 (clone SK3)was validated here http://www.bdbiosciences.com/us/applications/research/t-cell-immunology/th-1-cells/surface-markers/human/buv395-mouse-anti-human-cd4-sk3-also-known-as-leu3a/p/563550

CD8-BUV805 (clone SK1) was validated here http://www.bdbiosciences.com/eu/reagents/research/antibodies-buffers/immunology-reagents/anti-human-antibodies/cell-surface-antigens/buv805-mouse-anti-human-cd8-sk1/p/612890. This product is now discontinued
1A7 Anti-idiotype to detect GD2-CAR was first validated here Sen et al J Immunother 1998 and further utilized and validated in multiple publications (Long AH et al, Nat Med 2015; Alfonso M, J Immunol 2002; Mount CW, Nat Med 2018)
CD19-Idiotype provided by Laurence Cooper was validated here https://www.ncbi.nlm.nih.gov/pmc/articles/PMC3585808/ and further utilized in multiple publications (Lee DW, The Lancet 2015; Long AH, Nat Med 2015; Kochenderfer JN, J Clin Oncol 2015; Fraietta JA, Nat Med 2018)
c-Jun (60A8), IRF4(4964), JunB(C37F9), BATF(D7C5), were validated by manufacturer (https://www.cellsignal.com) as well as by our lab using CRISPR-Cas9-edited human primary T cells followed by western blotting and/or flow cytometry.
BATF3 (AF7437) was validated by our lab using CRISPR-Cas9-edited human primary T cells followed by western blotting, as well as here https://www.rndsystems.com/products/human-batf3-antibody_af7437.
GAPDH (D46CR) was validated here https://www.cellsignal.com/products/primary-antibodies/gapdh-d4c6r-mouse-mab/97166?N=4294956287&Ntt=gapdh&fromPage=plp
b-Actin-HRP (clone AC-15) was validated here https://www.sigmaaldrich.com/catalog/product/sigma/a3854?lang=en&region=US
P-c-JunSer73 (D47G9) was validated in our lab using CRISPR-Cas9-edited human primary T cells and overexpression vectors followed by western blotting. Further validation here https://www.cellsignal.com/products/primary-antibodies/phospho-c-jun-ser73-d47g9-xp-rabbit-mab/3270.
Histone 3 (1B1B2) was validated here https://www.cellsignal.com/products/primary-antibodies/histone-h3-1b1b2-mouse-mab/14269.

Eukaryotic cell lines

Policy information about cell lines

Cell line source(s)	Nalm6-GL was originally provided by Steve Grupp (CHOP). EW8 and TC32 were provided by Lee Helman (NCI). The 143b line was provided by C. Khanna (NCI, NIH); Kelly from C. Thiele (NCI, NIH); 293GP line by the Surgery Branch (NCI). 293T cells were obtained from the American Type Culture Collection (ATCC, Manassas)
Authentication	STR DNA profiling of all cell lines is conducted by Genetica Cell Line testing once per year.
Mycoplasma contamination	Before using for in vivo experiments, cell lines are tested with MycoAlert detection kit (Lonza). All cell lines tested negative.
Commonly misidentified lines (See ICLAC register)	None of the cell lines used in this study are included in the commonly misidentified cell lines registry.

Animals and other organisms

Policy information about studies involving animals; ARRIVE guidelines recommended for reporting animal research

Laboratory animals	6-8 week old male or female NOD/SCID/IL2Rg (NSG) mice were used for all in vivo experiments.
Wild animals	The study did not involve wild animals.
Field-collected samples	The study did not involve samples collected from the field.

Human research participants

Policy information about studies involving human research participants

Population characteristics	Buffy coats from anonymous healthy (male and female human, ages 30-50) were purchased from the Stanford University Blood Bank.
Recruitment	Written informed consent was obtained from all healthy donors.

ChIP-seq

Data deposition

☒ Confirm that both raw and final processed data have been deposited in a public database such as GEO.

☒ Confirm that you have deposited or provided access to graph files (e.g. BED files) for the called peaks.

Data access links *May remain private before publication.*	GEO Accession number: GSE136853
Files in database submission	*Provide a list of all files available in the database submission.*
Genome browser session (e.g. UCSC)	http://genome.ucsc.edu/s/snagara/Lynn%20et%20al%20enhanced%20CAR%2DT%20ChIP%2Dseq

Methodology

Replicates	ChIP-seq was performed in both JUN and Control (HA only) CAR-T cells in two biological replicates. Each replicate was a distinct viral transduction.
Sequencing depth	All ChIP-seq experiments were performed as paired-end sequencing at 2x75 bp length. Unique reads: ha-1-inp 89644144 ha-1-irf4 68466420 ha-1-jun 45203466 ha-2-inp 61388074 ha-2-irf4 39513462 jun-1-inp 61213392 jun-1-irf4 55079410 jun-1-jun 46053188 jun-2-inp 54899776 jun-2-irf4 50793788 jun-2-jun 42178818
Antibodies	JUN antibody: Active Motif, cat. no. 39309 IRF4 antibody: Abcam, cat. no. ab101168, lot. no. GR139704-21
Peak calling parameters	Reads were mapped using bowtie2 version 2.2.4 with the --very-sensitive flag. Peaks were called using MACS2 version 2.1.1.20160309 callpeak. HA-1 IRF4 and JUN peaks were called over ha-1-inp.sort.rmdup.bam HA-1 IRF4 peaks were called over ha-2-inp.sort.rmdup.bam JUN-1 IRF4 and JUN peaks were called over jun-1-inp.sort.rmdup.bam JUN-2 IRF4 and JUN peaks were called over jun-2-inp.sort.rmdup.bam
Data quality	ChIP peak enrichment was calculated using ENCODE QC parameters. Briefly, peak enrichment quality control was performed by downsampling bam files to 20 million reads using picardtools DownsampleSam and calling peaks again. ChIP and input coverage at these peaks was calculated using HOMER annotatePeaks.pl in 1 bp bins for 5 kb flanking each peak center. Enrichment at each base pair was calculated as (ChIP coverage/input coverage) and overall peak enrichment was defined as the maximum enrichment in the 500 bp flanking the peak center. Sample / Number of peaks called / Peak enrichment: ha-1-irf4 / 52270 / 5.96 ha-1-jun / 1712 / 1.61 ha-2-irf4 / 55087 / 9.59 jun-1-irf4 / 43398 / 5.80 jun-1-jun / 7857 / 3.35 jun-2-irf4 / 43639 / 8.90 jun-2-jun / 9703 / 3.39
Software	Sequencing adaptors were trimmed using cutadapt version 1.11 and aligned to the hg19 reference genome using bowtie2 version 2.2.4 with the --very-sensitive flag. Aligned reads with quality less than 10 removed and remaining reads were sorted using samtools version 1.2. PCR duplicates were removed using picardtools version 1.128 MarkDuplicates. For JUN ChIP-Rx, reads were first aligned to the hg19 genome and unmapped reads were mapped again to the dm6 Drosophila genome. Drosophila spike-in reads were filtered and deduplicated using the same parameters as described above. Sample H3K27me3 ChIP-seq were then normalized to reference-adjusted reads per million (RRPM), with normalization factor Nd = 1,000,000/(number of unique Drosophila reads) used to make bigwig files for visualization. For track visualization, each bam file was normalized to one million reads (rpm) or RRPM for JUN ChIP using bedtools version 2.19.1 genomecov -bg -split and then converting to bigwig format with bedGraphToBigWig. Tracks were displayed using the UCSC genome browser. Peaks were called using macs2 version 2.1.1.20160309 callpeak over input controls. Correlation plots were generated by counting reads within merged peaks using bedtools multicov. Enrichment plots were generated using HOMER by counting reads in 5 bp bins surrounding peak centers.

Flow Cytometry

Plots

Confirm that:

☐ The axis labels state the marker and fluorochrome used (e.g. CD4-FITC).

☒ The axis scales are clearly visible. Include numbers along axes only for bottom left plot of group (a 'group' is an analysis of identical markers).

☐ All plots are contour plots with outliers or pseudocolor plots.

☐ A numerical value for number of cells or percentage (with statistics) is provided.

Methodology

Sample preparation	Up to 1 million T cells from culture were washed with PBS + 2% FBS (FACS Buffer), labeled in 100uL FACS Buffer containing the relevant antibodies, and incubated at 4C in the dark for 20 minutes. Samples were washed 2X in 1mL FACS Buffer before running.

Instrument	BD LSRFortessa X-20
Software	FACSDiva for collection and FlowJo for analysis.
Cell population abundance	*Describe the abundance of the relevant cell populations within post-sort fractions, providing details on the purity of the samples and how it was determined.*
Gating strategy	All samples are gated on FSC/SSC lymphocyte populations, single cells (Using FSC-W/FSC-H and SSC-W/SSC-H), then either CD4 or CD8+. Frequency of positive gates is determined using an isotype or FMO control.

☐ Tick this box to confirm that a figure exemplifying the gating strategy is provided in the Supplementary Information.